Molecular Mechanisms of BTK Dependency

in Primary CNS Lymphoma

by

Sarah Shiann Tang

A dissertation presented to the faculty of the

Louis V. Gerstner, Jr. Graduate School of Biomedical Sciences

Memorial Sloan Kettering Cancer Center

in partial fulfillment of the requirements for the degree of

Doctor of Philosophy

New York, NY

July, 2021

_____   _____

Ingo Mellinghoff, M.D.   Date
Dissertation Mentor

DEDICATION

This thesis is dedicated to my parents, Hal Tang and Ha Huynh. I could not have accomplished this without your unconditional love and support. I will be forever grateful.

ABSTRACT

Ibrutinib, the first-in-class inhibitor of Bruton tyrosine kinase (BTK), has elicited excellent responses in relapsed/refractory (r/r) primary central nervous system lymphoma (PCNSL) patients, suggesting a strong dependency on BTK. To further understand the effectors that drive the survival and pathogenesis of PCNSL downstream of BTK, we investigated the molecular response to BTK inhibition and defined a signature of BTK-regulated genes. We established novel PCNSL patient-derived xenograft (PDX) models that were sensitive to ibrutinib and utilized the models to uncover the BTK-regulated transcriptome, which included genes related to NF-κB/TNFα and protein translation. We also modeled acquired ibrutinib resistance because many patients developed resistance. We identified candidate resistance mutations in PLCG2 and CARD11, but not BTK, in both PCNSL cell lines and PCNSL patients in our study. CARD11 mutation was associated with shorter progression-free survival (PFS) in PCNSL patients on ibrutinib, indicating a correlation between CARD11 mutation and resistance. We found that CARD11 mutations restored signaling through MALT1 and mTOR, but that only inhibition of mTOR combined with ibrutinib effectively induced cell death in CARD11-mutant cells. Thus, we have demonstrated that BTK regulates both NF-κB/TNFα and protein translation in PCNSL models, and that CARD11 mutation-mediated ibrutinib resistance can be overcome with combined ibrutinib and mTOR inhibitor treatment.

BIOGRAPHICAL SKETCH

Sarah Tang was born on May 26, 1993 in the city of Orange, CA to her parents, Hal Tang and Ha Huynh. Her father, Hal, is incredibly hardworking and humble. Her mother, Ha, is very dedicated to family and ensures that we feel loved and supported. Sarah has 2 sisters, Kelly and Elaine, who have always pushed her to face challenges, be brave, and follow her heart. Growing up, Sarah loved biology and was fascinated by the study of human disease. She went on to earn a Bachelor of Science in Immunology and Microbiology at the University of California, Irvine. While in Irvine, Sarah studied in a cancer immunology laboratory and became inspired to pursue a PhD. She made the cross-country move to New York City to attend the Gerstner Sloan Kettering Graduate School at Memorial Sloan Kettering Cancer Center, a world-class institution for cancer research. Sarah also fulfilled her dreams of living in the big city. She joined the laboratory of Ingo Mellinghoff, where she met brilliant scientists and clinicians who make a positive impact on the world each and every day. Sarah has grown so much over the years, both professionally and personally, and she is ready to take on the next chapter in her life.

ACKNOWLEDGEMENTS

former Mellinghoff lab member, Wan-Ying Hsieh, who has been a close friend and mentor to me. I greatly admire her intelligence and strength, and am very appreciative of the friendship we share both inside and outside of the lab.

I would like to thank the Gerstner Sloan Kettering Graduate School, especially Ken Marians, Michael Overholtzer, Linda Burnley, Thomas Magaldi, and David McDonagh, for always checking in to make sure I am on track to graduate and that I am happy in the lab. I would also like to thank my wonderful classmates, who have shared with me so many memories over the years.

I would like to thank all my former mentors, especially David Fruman and Scott Lee, who first introduced me to the world of cancer research and inspired me to pursue a PhD. I am so thankful to have support from such amazing role models.

Most importantly, I would like to thank all my friends and family who have stood beside me on this long but rewarding journey. My parents, Hal Tang and Ha Huynh, my sisters, Kelly Woo and Elaine Tang, and my partner, Wilson Hsieh, have been my rock during this time in graduate school. There are no words to describe how thankful I am to have their unending love and support.

Last but not least, I would like to pay tribute to all the mice that made this research possible.

TABLE OF CONTENTS

LIST OF TABLES

LIST OF FIGURES

LIST OF ABBREVIATIONS

ABC: Activated B cell subtype of DLBCL

BCR: B cell receptor

BTK: Bruton tyrosine kinase

CARD11: Caspase recruitment domain family member 11

CD79B: B-cell antigen receptor complex-associated protein beta chain

CLL: Chronic lymphocytic leukemia

CNS: Central nervous system

CSF: Cerebral spinal fluid

DLBCL: Diffuse large B cell lymphoma

GCB: Germinal center B cell subtype of DLBCL

GSEA: Gene set enrichment analysis

Ibrutinib: Ibr

IC: Intracranial

IHC: Immunohistochemistry

IP: Intraperitoneal

IV: Intravenous

MALT1: Mucosa-associated lymphoid tissue lymphoma translocation protein 1

MCL: Mantle cell lymphoma

mTOR: Mammalian target of rapamycin

mTORC1: Mammalian target of rapamycin complex 1

mTORC2: Mammalian target of rapamycin complex 2

MYD88: Myeloid differentiation primary response 88

MZL: Marginal zone lymphoma

NF-κB: Nuclear factor kappa light chain enhancer of activated B cells

NGC: Non-germinal center B cell subtype of DLBCL

PCNSL: Primary central nervous system lymphoma

PDX: Patient-derived xenograft

PFS: Progression-free survival

PI3K: Phosphoinositide 3-kinase

PLCG2: Phospholipase C-γ-2

r/r: Relapsed/refractory

Rapamycin: Rap

SC: Subcutaneous

SCM-02-138: SCM

SCNSL: Secondary central nervous system lymphoma

SLL: Small lymphocytic leukemia

TLR: Toll-like receptor

TNFα: Tumor necrosis factor α

WM: Waldenstrom macroglobulinemia

CHAPTER 1: INTRODUCTION

Primary Central Nervous System Lymphoma (PCNSL)

Primary central nervous system lymphoma (PCNSL) is a rare, aggressive non-Hodgkin lymphoma that presents most often in patients over the age of 60 and has an incidence of 0.5 per 100,000 individuals per year in the United States (Grommes & DeAngelis, 2017). PCNSL arises in the central nervous system (CNS), including the brain, cerebral spinal fluid (CSF), spinal cord, and eye, and does not typically metastasize outside of the CNS.

The majority (>90%) of PCNSL is clinically categorized as diffuse large B cell lymphoma (DLBCL). The other 10% of PCNSL that is not DLBCL are T cell lymphomas, Burkitt lymphomas, or low-grade lymphomas (Grommes & DeAngelis, 2017; Lim et al., 2011). DLBCL that originally presents systemically (referred to as non-CNS DLBCL) can relapse in the CNS, and this is called secondary CNS lymphoma (SCNSL). SCNSL occurs in about 1-10% of non-CNS DLBCL cases (Rocha et al., 2013).

Differences between PCNSL and non-CNS DLBCL

Although PCNSL is clinically categorized as DLBCL, there are unique features that distinguish PCNSL from non-CNS DLBCL. One obvious feature is that by definition PCNSL arises and grows exclusively within the CNS. This is intriguing since the CNS is considered to be an immune-privileged space. However, a recent study identified B cells and progenitors in the meninges of

non-tumor bearing mice and rats, suggesting that the CNS may support normal B cell development (Schafflick et al., 2021). There has also been evidence that the CNS can support certain immune cell processes under inflammatory conditions. For example, CNS homing factors, ectopic lymphoid follicle formation, and B cell differentiation have been detected in the meninges of patients with multiple sclerosis and other neurological diseases (Uccelli, Aloisi, & Pistoia, 2005). It is conceivable that these processes may also occur in PCNSL, but there is no evidence to support this yet.

How CNS tropism might be linked to PCNSL pathogenesis has been explored. One idea is that the B cell receptors (BCR) of PCNSL cells interact with CNS-specific self-antigens that activate BCR signaling. A previous study expressed recombinant antibodies from immunoglobulin heavy chain variable (IGHV) gene segments found in PCNSL, and found that the antibodies interacted with galectin-3, a protein secreted by CNS cells only in the presence of PCNSL tumor cells (Manuel Montesinos-Rongen et al., 2015). This suggested that PCNSL tumor interaction with galectin-3 might be important for disease pathogenesis. Another study reported that B cell activating factor of the tumor necrosis factor family (BAFF) is produced by astrocytes in the normal brain, and that BAFF receptors were highly expressed in some PCNSL tumors, suggesting that BAFF could bind to BAFF receptors on PCNSL tumor cells to activate signaling and promote survival in the CNS microenvironment (Krumbholz et al., 2005).

Genetic Profiling of PCNSL Tumors

In recent years, our understanding of PCNSL has increased enormously with systematic efforts to genetically profile tumors at Memorial Sloan Kettering Cancer Center (MSKCC) (Cerami et al., 2012; Gao et al., 2013). Targeted DNA sequencing of PCNSL tumors revealed recurrent mutations in myeloid differentiation primary response 88 (MYD88) and B-cell antigen receptor complex-associated protein beta chain (CD79B) in 58% and 41% of patients, respectively (Grommes et al., 2017). MYD88 encodes an adaptor protein downstream of the Toll-like receptor (TLR), and CD79B encodes a B cell receptor (BCR) co-signaling molecule. These proteins converge on Bruton tyrosine kinase (BTK), a central signaling node in the BCR pathway.

Other recurrently mutated genes in PCNSL included PIM1 (56%), BTG2 (36%), MLL2 (28%), PRDM1 (27%), MSH3 (27%), TBL1XR1 (23%), TOX (20%), IRF4 (17%), CREBBP (17%), CARD11 (13%), and TNFAIP3 (14%) (Grommes et al., 2017). TBL1XR1, IRF4, CARD11, and TNFAIP3 also encode proteins involved in signaling through the BCR/TLR pathways, further pointing to a role for these pathways in PCNSL pathogenesis. Several of these recurrently mutated genes, namely PIM1, BTG2, PRDM1, TOX, and IRF4 were also targets of aberrant somatic hypermutation (SHM) (Grommes et al., 2017). Aberrant SHM was determined based on the proximity of the mutation to the transcription start site, mutation presence within WGYR motifs, and the specific mutation type (transition vs. transversion; C/T vs. A/G) (Khodabakhshi et al., 2012). Mutations resulting from aberrant SHM are not typically considered to be drivers of disease,

but in some cases may contribute to disease pathogenesis (Khodabakhshi et al., 2012; M. Montesinos-Rongen, Van Roost, Schaller, Wiestler, & Deckert, 2004; Pasqualucci et al., 2001; Schneider, Pasqualucci, & Dalla-Favera, 2011). Curiously, the most frequently mutated genes in PCNSL are observed less frequently in non-CNS DLBCL (MYD88: 16.8%, CD79B: 16.5%, PIM1: 22.5%, BTG2: 13%), perhaps suggesting different disease dependencies (Grommes et al., 2017).

Analysis of copy number alterations in PCNSL tumors revealed frequent loss of chromosomes 6p, 6q, and 9p (CDKN2A) and gain of chromosomes 3q (NFKBIZ), 18q (BCL2), and 19q (EPN1, FIZ1, ZNF579) (B. Chapuy et al., 2016). The chromosome losses (6p, 6q, 9p) were noticeably more frequent in PCNSL compared to non-CNS ABC DLBCL, while the frequencies of chromosome gains appeared to be similar (B. Chapuy et al., 2016).

PCNSL Classification

DLBCL is a highly heterogeneous disease with 2 major subtypes defined by gene expression profiling and presumed cell of origin (Alizadeh et al., 2000). The 2 subtypes are the germinal center B cell (GCB) subtype and the activated B cell (ABC) subtype, also known as the non-germinal center (NGC) subtype. The NGC subtype is more aggressive and resistant to chemotherapy, resulting in poorer patient outcomes compared to the GCB subtype (Alizadeh et al., 2000). In the clinic, the Hans classification is often used to classify DLBCL tumors into GCB or NGC subtypes based on immunohistochemistry staining for BCL-6,

CD10, and MUM-1 (Hans, 2004). Based on this classification, nearly all PCNSL are the NGC subtype, the more aggressive and chemo-resistant DLBCL subtype.

Considering that DLBCL is such a heterogeneous disease, there have been more recent efforts to redefine DLBCL subtypes based on genetic alterations. In one study, investigators performed whole exome sequencing in a cohort of 304 DLBCL patients to identify genetic mutations, copy number alterations, and structural variants, which were used to determine clusters of DLBCL. They found 5 clusters (C1, C2, C3, C4, C5), as well as a C0 cluster, which comprised samples without defining genetic alterations (Bjoern Chapuy et al., 2018). Key features of the clusters were as follows: C1 cluster had BCL6 structural variants and NOTCH2 and NF-κB pathway mutations; C2 cluster had TP53 inactivation and various chromosomal losses (RB1, CDKN2A) or gains (MCL1); C3 cluster had BCL2 mutations with structural variant, mutations in chromatin modifiers, and PTEN mutation or loss; C4 cluster had histone mutations, and NF-κB, JAK/STAT, and Ras pathway mutations; C5 cluster had gain of chromosome 3p, 3q, 18p, and 18q (BCL2) and mutations in CD79B, MYD88, ETV6, and PIM1. CNS DLBCL was classified in the C5 cluster. Clusters C1 and C5 were mostly NGC DLBCL, while C3 and C4 were GCB DLBCL (Bjoern Chapuy et al., 2018).

In another study, investigators developed an algorithm called LymphGen to classify DLBCL into subtypes based on genetic alterations (Schmitz et al., 2018; Wright et al., 2020). They identified 6 subtypes with key genetic features: 1) MCD subtype had MYD88 and CD79B mutation, BCL2 gain, and CDKN2A

loss; 2) BN2 subtype had NOTCH2 mutation, BCL6 alteration, and NF-κB pathway mutations; 3) EZB subtype had mutations in epigenetic modifiers and PTEN alteration; 4) ST2 subtype had SGK1 and TET2 mutation; 5) A53 had TP53 alteration; 6) N1 had NOTCH1 mutation. PCNSL tumors were classified as the MCD subtype. MCD, N1, and A53 subtypes were largely NGC DLBCL, while ST2 and EZB subtypes were GCB DLBCL (Wright et al., 2020).

The B cell receptor and Toll-like receptor pathways

The BCR signaling pathway (Figure 1.1) is activated upon engagement of antigen, which leads to CD79A and CD79B phosphorylation on tyrosine residues within the immunoreceptor tyrosine-based activation motifs (ITAM) (Gold, Law, & DeFranco, 1990; Gold, Matsuuchi, Kelly, & DeFranco, 1991; Pao, Famiglietti, & Cambier, 1998). Phosphorylated ITAMs recruit Src homology 2 (SH2) domain-containing proteins to the plasma membrane to transduce the signal. These proteins include the adaptor B-cell linker protein (BLNK) and Syk and Lyn tyrosine kinases. BTK is also recruited to the plasma membrane via interaction of its pleckstrin homology (PH) domain with phosphatidylinositol (3,4,5)-trisphosphate (PIP3), which is generated by phosphoinositide 3-kinase (PI3K) phosphorylation of phosphatidylinositol (4,5)-bisphosphate (PIP2) (Saito, Scharenberg, & Kinet, 2001). With these proteins brought into close proximity at the plasma membrane, Syk and Lyn phosphorylate BTK at Y551 (kinase domain) and BTK then auto-phosphorylates at Y223 (Src homology 3 (SH3) domain) for full activation (Baba et al., 2001; Kurosaki & Kurosaki, 1997). BTK also dimerizes
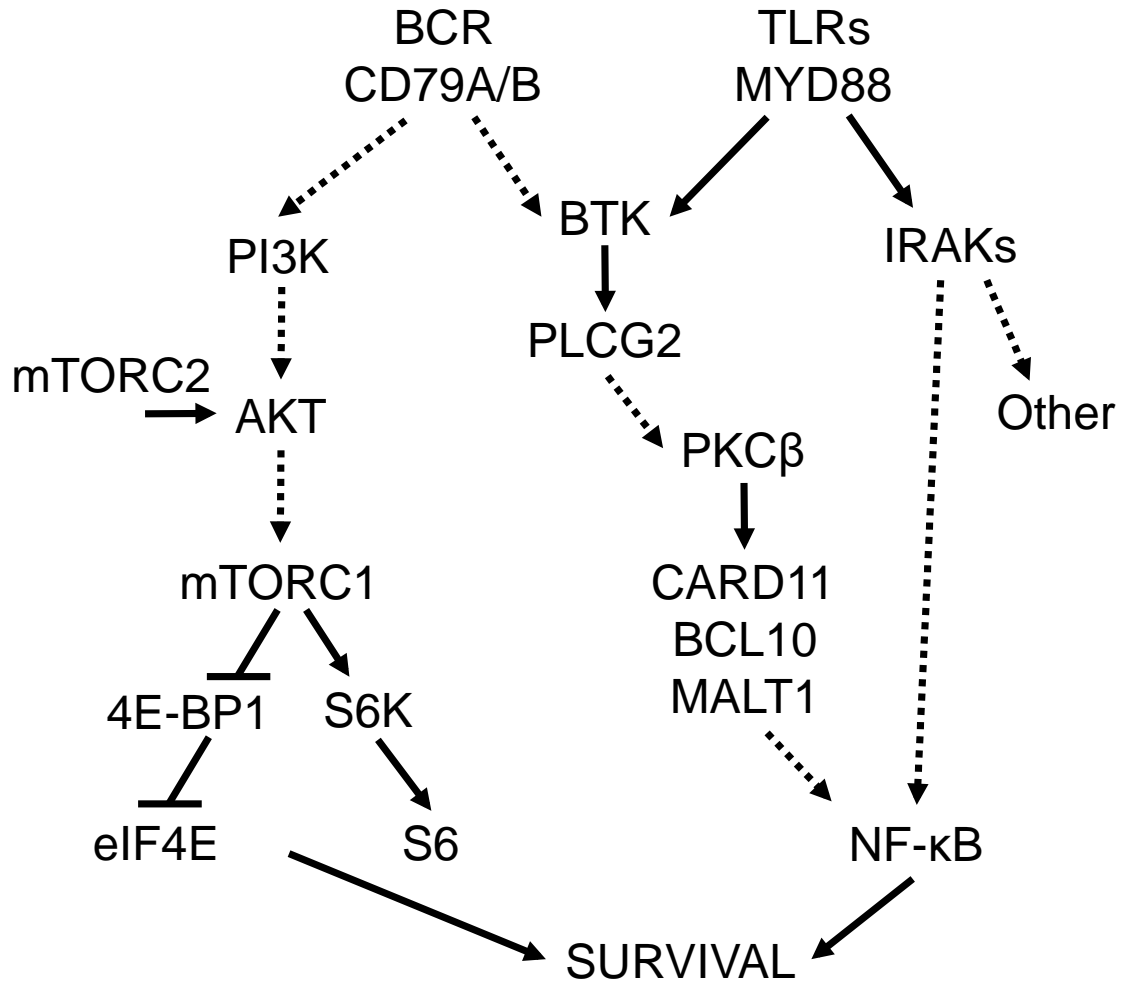
Figure 1.1. B cell receptor signaling and related pathways. This cartoon shows a simplified illustration of the BCR signaling network through BTK and PI3K as well as the convergence of the BCR pathway with the TLR pathway at BTK. The solid arrows indicate direct interactions while the dotted arrows indicate indirect interactions between proteins or processes. A detailed description of these pathways is included in the text.

via its PH and Tec homology (TH) domains (Chung et al., 2019). Lyn can have either activating or inhibitory effects on BCR signaling depending on the context (Y. Xu, Harder, Huntington, Hibbs, & Tarlinton, 2005). Activated BTK phosphorylates its substrate, phospholipase C-γ-2 (PLCG2), which cleaves PIP2 into the second messengers, inositol trisphosphate (IP3) and diacylglycerol (DAG) (Kim, Sekiya, Poulin, Bae, & Rhee, 2004; Rhee & Bae, 1997). IP3 is very unstable and is rapidly dephosphorylated into inositol bisphosphate (IP2) and inositol monophosphate (IP1).

Increased levels of inositol phosphates trigger intracellular calcium release from the endoplasmic reticulum into the cytoplasm (Berridge, 1993). This increased calcium flux leads to phosphoinositide-dependent kinase-1 (PDK-1)-mediated phosphorylation and activation of protein kinase C β (PKCβ), which phosphorylates caspase recruitment domain family member 11 (CARD11) (Dutil, Toker, & Newton, 1998). CARD11 is a large scaffolding protein with an auto-inhibitory domain that keeps the protein in an inactive conformation. When PKCβ phosphorylates CARD11 in its auto-inhibitory domain, the auto-inhibition of CARD11 is released, converting CARD11 into an open, active conformation (Z. Wang et al., 2019). CARD11 oligomerizes and recruits B-cell lymphoma 10 (BCL10) and mucosa-associated lymphoid tissue lymphoma translocation protein 1 (MALT1), forming a signaling complex called the CBM (Ruland & Hartjes, 2018). Within the CBM complex, BCL10 and MALT1 form heterodimers and assemble into modules that help recruit other proteins. MALT1 is a paracaspase, a caspase-like protein, with protease activity that is known to cleave at least 9

substrates including itself, BCL10, regulators of nuclear factor kappa light chain enhancer of activated B cells (NF-κB), and mRNA repressor proteins, such as Roquin 1/2 (Ruland & Hartjes, 2018).

Additional proteins recruited to the CBM complex include mitogen-activated protein kinase kinase kinase 7 (TAK1), IκB kinase (IKK), tumor necrosis factor receptor-associated factor 6 (TRAF6), linear ubiquitin chain assembly complex (LUBAC) including HOIL-1L interacting protein (HOIP), and cellular inhibitor of apoptosis protein (cIAP). Both TRAF6 and HOIP have E3 ubiquitin ligase activity and can ubiquitinate TAK1 and IKK (Ruland & Hartjes, 2018). TAK1 is thought to phosphorylate and activate IKK, which subsequently phosphorylates inhibitor of nuclear factor kappa B (IκBα) and targets it for proteasomal degradation. The function of IκBα is to bind NF-κB and hide its nuclear localization signal, thereby keeping NF-κB in the cytoplasm and inhibiting NF-κB from performing its function (Beg et al., 1992). The degradation of IκBα thereby activates NF-κB by allowing it to enter the nucleus to regulate gene transcription. NF-κB is a transcription factor that regulates the expression of hundreds of genes involved in immune response, cytokine signaling, cell proliferation, and apoptosis (Q. Zhang, Lenardo, & Baltimore, 2017).

Like the BCR pathway, the TLR pathway (Figure 1.1) can also activate BTK and NF-κB (Jefferies et al., 2003). There are multiple different TLRs that are localized either at the plasma membrane or endosomal membranes within the cell. TLRs contain Toll/interleukin-1 receptor (TIR) homology domains, and all TLRs except TLR3 recruit the MYD88 adaptor protein via the TIR domain

(O'Neill, Golenbock, & Bowie, 2013). MYD88 also has a death domain, allowing it to interact with interleukin-1 receptor associated kinases (IRAKs) (Loiarro et al., 2009). There are 4 IRAK proteins that mediate downstream signaling through not only NF-κB, but also through other transcription factors like cAMP-response element binding protein (CREB), activator protein-1 (AP-1), and interferon-regulatory factors 3/7 (IRF3/7) (O'Neill et al., 2013; Rhyasen & Starczynowski, 2014). MYD88 with the L265P hotspot mutation has been shown to aberrantly bind and hyper-activate BTK in Waldenstrom macroglobulinemia (G. Yang et al., 2013). Mutant MYD88 has also been reported to activate Syk and Hck tyrosine kinases to promote BCR signaling in DLBCL (Munshi et al., 2020). This gain of function mutation in MYD88 has therefore provided cells with an alternative mechanism of BCR pathway activation and cell survival that is independent from normal TLR signaling through IRAKs.

The BCR can also activate the PI3K pathway (Figure 1.1), which mediates cell growth, proliferation, and survival (Srinivasan et al., 2009). PI3K phosphorylates PIP2 to generate PIP3, which recruits PH domain-containing proteins, such as PDK-1 and protein kinase B (AKT), to the plasma membrane. PDK-1 phosphorylates AKT at T308, which then allows mammalian target of rapamycin complex 2 (mTORC2) to subsequently phosphorylate AKT at S473 to fully activate AKT (Alessi et al., 1997; Sarbassov, Guertin, Ali, & Sabatini, 2005). AKT has many substrates and regulates various cellular processes. One substrate is proline-rich AKT substrate of 40 kDa (PRAS40), which is a negative regulator of mammalian target of rapamycin complex 1 (mTORC1) (L. Wang,

Harris, Roth, & Lawrence, 2007). AKT phosphorylation of PRAS40 at T246 promotes its interaction with 14-3-3 proteins and releases its inhibitory effects on mTORC1, thereby activating mTORC1. AKT can also activate mTORC1 by inhibiting tuberous sclerosis complex subunit 1/2 (TSC1/2), which inhibits Rheb, an activator of mTORC1. mTORC1 has 2 well-studied effectors, ribosomal protein S6 kinase (S6K) and eukaryotic translation initiation factor 4E-binding protein 1 (4E-BP1). S6K phosphorylates ribosomal protein S6 and is involved in ribosome biogenesis, while both S6K and 4E-BP1 are critical regulators of protein translation (Chauvin et al., 2014; Holz, Ballif, Gygi, & Blenis, 2005; Mamane, Petroulakis, LeBacquer, & Sonenberg, 2006). mTORC1 is known to integrate various signals from the intracellular environment and promote cell growth and survival. In addition to being activated by BCR signaling, the PI3K/AKT/mTOR pathway can also be activated by growth factor receptors, such as the epidermal growth factor receptor (EGFR), and has been implicated in many hematological malignancies and solid tumors (Fruman et al., 2017).

Treatments for PCNSL

The key features of PCNSL tumors, including angiocentric growth, high proliferation, and infiltration in deep brain regions, add to the complexity of disease treatment. Surgical resection of the tumor is typically not feasible. Due to the rarity of the disease and limited enrollment of certain clinical trials, it has been challenging to establish a standard treatment regimen for PCNSL patients (Schaff, Ambady, Doolittle, & Grommes, 2021). The exception is that it is

generally agreed that high dose-methotrexate (HD-MTX) should be used as part of induction therapy. HD-MTX is generally prescribed with additional chemotherapies and rituximab for induction therapy. Consolidation therapy consists of various chemotherapies, whole brain radiation therapy (WBRT), and/or high dose chemotherapy with autologous stem cell transplantation for younger patients. Despite high response rates to induction and consolidation therapies, 10-15% of patients still have primary refractory disease and the median time to relapse is 10-18 months (Grommes & DeAngelis, 2017). Treatments for relapsed patients are limited but typically include WBRT, HD-MTX, chemotherapies, and rituximab.

The development of BCR pathway inhibitors, particularly BTK inhibitors, in the past decade has proved to be very promising for the treatment of many B cell malignancies. Ibrutinib is the first-in-class BTK inhibitor and blocks BTK activity by covalently binding to cysteine 481 (C481) within the active site of BTK. Ibrutinib was first FDA-approved for the treatment of mantle cell lymphoma (MCL) in 2013, and has since then been FDA-approved for chronic lymphocytic leukemia (CLL), Waldenstrom macroglobulinemia (WM), small lymphocytic leukemia (SLL), and marginal zone lymphoma (MZL) (Jan A. Burger et al., 2015; Byrd et al., 2013; Noy et al., 2017; Treon et al., 2015; M. L. Wang et al., 2013). Our research group at MSKCC conducted a Phase 1 clinical trial to evaluate the effect of ibrutinib in relapsed/refractory (r/r) PCNSL patients and found that PCNSL patients responded very well to ibrutinib (Grommes et al., 2017; Lionakis et al., 2017). Ibrutinib has not yet been FDA-approved for r/r PCNSL, but has

been added to the National Comprehensive Cancer Network (NCCN) guidelines in 2018 for the treatment of r/r PCNSL. Moreover, clinical trials are currently ongoing to evaluate several ibrutinib-based combination therapies in PCNSL, including with rituximab and methotrexate (Grommes et al., 2019), immune-modulating agent lenalidomide (NCT03703167), PI3K inhibitor copanlisib (NCT03581942), and immune checkpoint inhibitors (Schaff et al., 2021).

Following the success of ibrutinib, several 2nd generation BTK inhibitors have been developed to target BTK with greater specificity in order to minimize toxicities observed with ibrutinib. Two such inhibitors are acalabrutinib and zanubrutinib, both of which inhibit BTK by binding irreversibly to C481. Both drugs have been FDA-approved for MCL, and only acalabrutinib has been FDA-approved for CLL patients thus far (Byrd et al., 2016; Song et al., 2020; M. Wang et al., 2018). Despite the initial success of ibrutinib, there are patients who progress on therapy, indicating the development of drug resistance. One mechanism of resistance that occurs frequently in CLL is mutation of BTK C481, the site at which these drugs bind (Woyach et al., 2017). To overcome BTK C481 mutation-mediated resistance, 3rd generation BTK inhibitors, such as pirtobrutinib, have been designed to reversibly bind BTK at a site other than C481 (Mato et al., 2021). Other mechanisms of resistance observed in B cell malignancies include gain of mutations in other BCR pathway genes, such as PLCG2 or CARD11, suggesting that re-activation of this pathway in one or more ways may contribute to ibrutinib resistance.

Introduction to Dissertation

Ibrutinib is very effective for the treatment of many B cell malignancies, suggesting strong dependencies on BTK. However, not all B cell malignancies respond to ibrutinib, indicating that BTK dependency is not observed by default in all B cells but rather has developed only in certain B cell cancers. Since PCNSL is very responsive to ibrutinib and thus is dependent on BTK, we aimed to further understand the BTK signaling pathway by determining the BTK-regulated transcriptome in PCNSL.

Although the initial response to ibrutinib was exceptional, many patients eventually acquired resistance. In CLL, MCL, and WM patients, mutations within the BCR pathway have been reported, but the specific genes and frequency of mutation in these genes appeared to differ between diseases. The ibrutinib resistance mechanisms in PCNSL still remain unknown.

Therefore, the aims of this dissertation are to 1) determine the molecular response to BTK inhibition in PCNSL models, and 2) elucidate the mechanisms of ibrutinib resistance to develop strategies to overcome resistance in PCNSL.

CHAPTER 2: MOLECULAR RESPONSE TO BTK INHIBITION

IN PCNSL

Introduction:

BTK is essential for many B cell functions, including development, differentiation, and signal transduction (de Weers et al., 1994). However, not all B cell malignancies responded to ibrutinib. For example, non-CNS DLBCL patients had only a 25% overall response rate to ibrutinib (NGC subtype: 37%, GCB subtype: 5%) (Wilson et al., 2015). This indicated that the B cell malignancies that did respond to ibrutinib, such as PCNSL, somehow developed a dependency on BTK. To further understand the pathway downstream of BTK that mediated the survival and pathogenesis of PCNSL, we aimed to define the BTK-regulated transcriptional program in this disease (Figure 2.1).

PCNSL and other B cell malignancies, such as CLL, MCL, and WM, all clinically responded very well to ibrutinib, but the mechanisms of BTK activation appeared to be somewhat unique in different diseases. For example, CLL patients had constitutive BCR activation mediated by the tumor microenvironment while BCR activation in MCL patients was partially linked to the tyrosine kinase Syk (Byrd et al., 2013; M. L. Wang et al., 2013). Neither CLL nor MCL patients had mutations in the BCR pathway. On the other hand, 90-95% of WM patients had mutations in MYD88 (Treon et al., 2015). PCNSL patients had frequent MYD88 and CD79B mutations, but patients without these mutations also responded well to ibrutinib, indicating that there were additional mechanisms
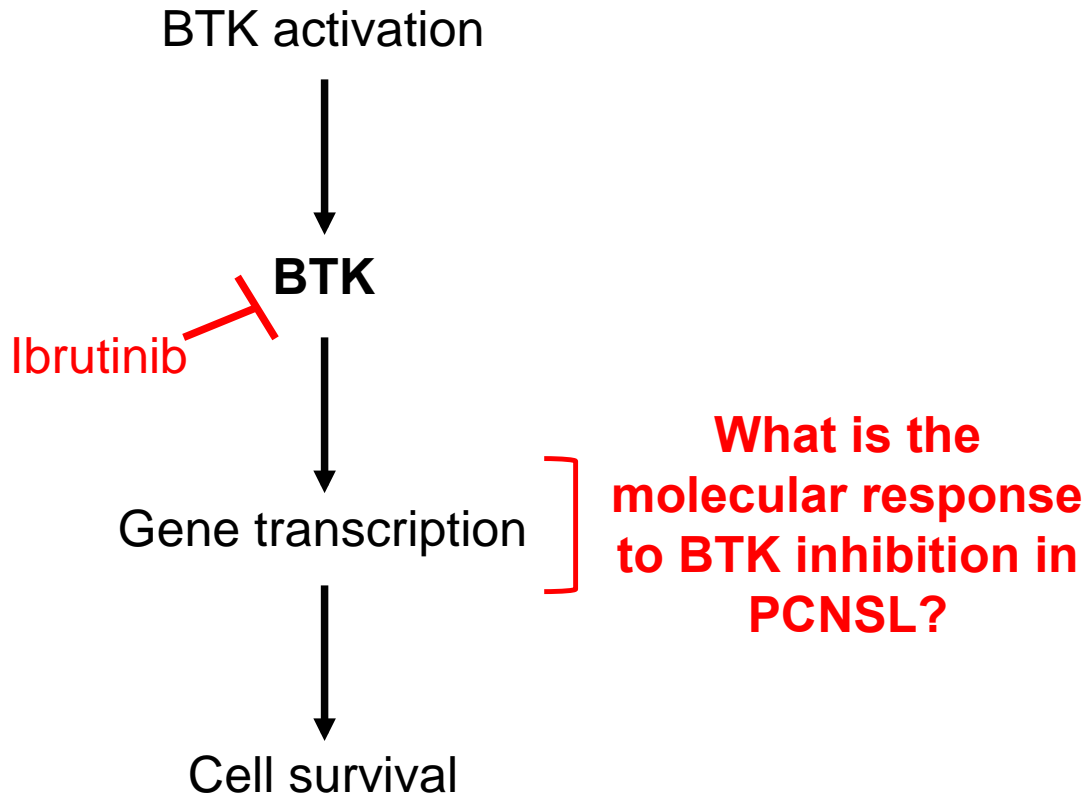
Figure 2.1. BTK dependency and molecular ibrutinib response in PCNSL.
This cartoon illustrates the goal of Chapter 2, which is to determine the molecular response to BTK inhibition in PCNSL.

of BTK activation in PCNSL. These different mechanisms of BTK activation hinted that there might also be unique transcriptional programs specifically regulated by BTK in distinct B cell malignancies.

In this chapter, we determined the PCNSL-specific molecular response to ibrutinib using novel patient-derived xenograft (PDX) models of PCNSL as well as PCNSL cell lines. We found that BTK strongly regulates not only NF-κB and tumor necrosis factor α (TNFα) but also protein translation pathways through Myc and mTORC1 in PCNSL models. Identifying these downstream effects of ibrutinib provided insight into the pathogenesis of PCNSL, and will aid in our understanding of how cells might restore components of these pathways in the development of drug resistance.

Results:

We have established 8 PCNSL PDX models from brain biopsies of newly diagnosed, previously untreated PCNSL patients (Table 2.1). The median age of patients was 68 years, and 5 patients were female. All patient tumors were positive for CD20 and negative for CD3.

Patient brain biopsies were first established in the mouse brain by intracranial injection (passage 1), and subsequently engrafted at intracranial (IC), subcutaneous (SC), intraperitoneal (IP), or intravenous (IV) sites to examine the ability of PDX tumors to grow in other organs of the mouse (Figure 2.2A). The tumor take was the highest when cells were injected intracranially, and 3 PDX models also grew subcutaneous tumors (Figure 2.2B). Mice with IC tumors

Patient ID	Biopsy Site	Age	Gender	Treatment Status	Tumor Immuno-phenotype
PCNS#6	Brain	85	F	Untreated	CD20 + CD3 -
PCNS#10	Brain	72	F	Untreated	CD20 + CD3 -
PCNS#11	Brain	64	M	Untreated	CD20 + CD3 -
PCNS#13	Brain	82	F	Untreated	CD20 + CD3 -
PCNS#14	Brain	62	F	Untreated	CD20 + CD3 -
PCNS#15	Brain	61	M	Untreated	CD20 + CD3 -
PCNS#16	Brain	62	F	Untreated	CD20 + CD3 -
PCNS#21	Brain	74	M	Untreated	CD20 + CD3 -

Table 2.1. Characteristics of PCNSL patients from which PDX models were derived. Patient brain biopsies were used to derive all PDX models. The patient age, gender, treatment status, and immuno-phenotype are shown. All PCNSL patients were newly diagnosed and did not receive any prior treatments. CD20 and CD3 were used to determine the immuno-phenotype.

A PCNSL patient brain biopsy → Establish in Mouse Intracranial (IC) – Passage 1 → Mouse Intracranial (IC) → Serial passage (IC); Mouse Subcutaneous (SC); Mouse Intraperitoneal (IP); Mouse Intravenous (IV)

B Tumor take (%) — IC, SC, IP, IV; PCNS#6, PCNS#10, PCNS#11, PCNS#13, PCNS#14, PCNS#15, PCNS#16, PCNS#21

C Survival of mice with intracranial (IC) tumors
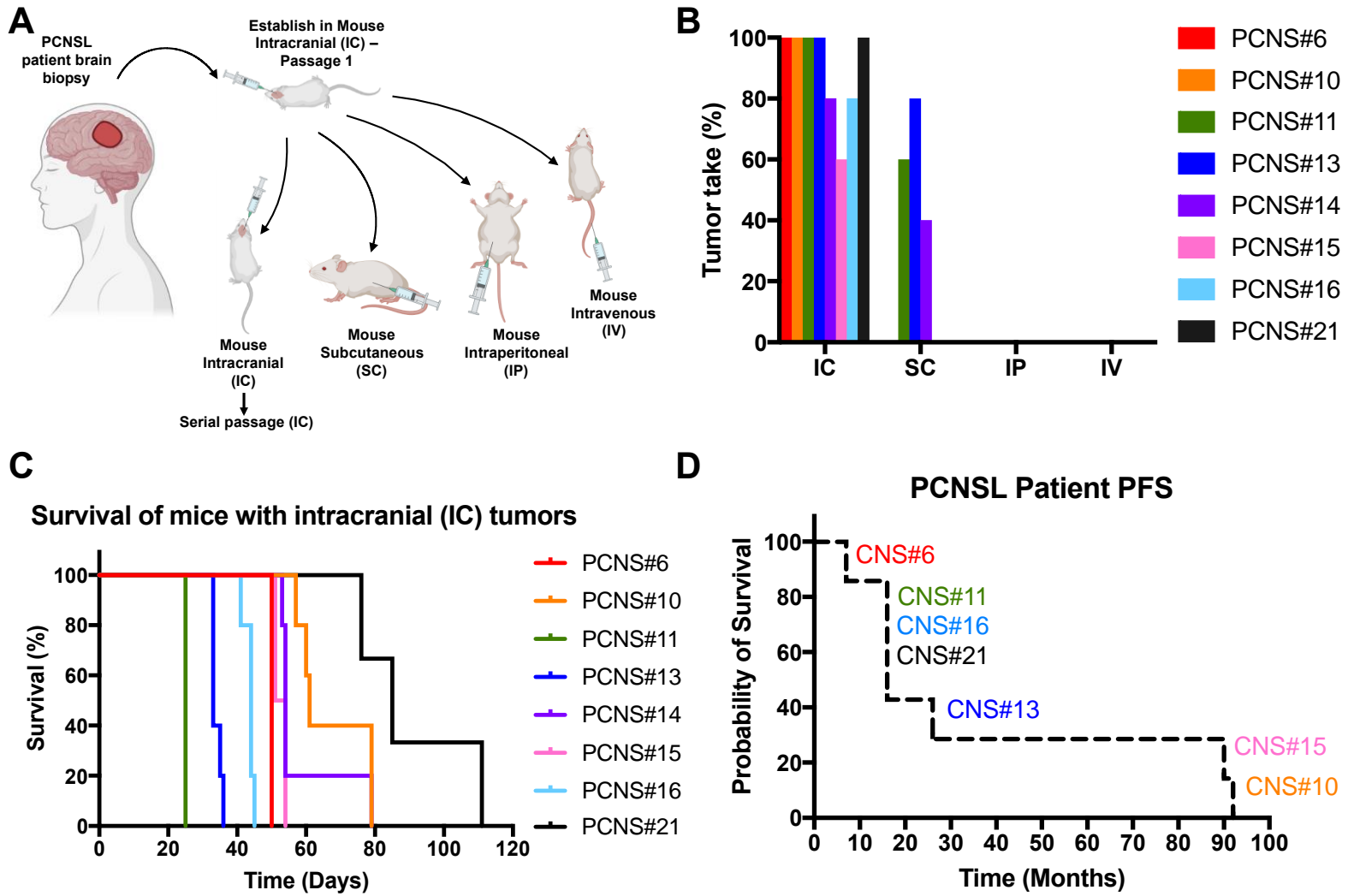
D PCNSL Patient PFS

(Figure 2.2 description is continued on the next page)

Figure 2.2 (continued)

Figure 2.2. PCNSL PDX tumors grow aggressively in the mouse brain. A) Workflow illustrating the initial establishment of cells from PCNSL patient brain biopsies in the mouse brain (passage 1) and subsequent engraftment of cells into different mouse organs. Cells engrafted at the intracranial site were serially passaged for further experiments. IC: intracranial, SC: subcutaneous, IP: intraperitoneal, IV: intravenous. Images were made in BioRender. **B)** Tumor takes in mice injected with cells at IC, SC, IP, and IV sites. Number of cells injected IC: 1×10^4 cells/mouse, SC: 1×10^6 cells/mouse, IP: 1×10^6 cells/mouse, IV: 2×10^6 cells/mouse. n=5 mice per site. **C)** Survival of mice with IC tumors at the 2nd passage. For PCNS#21, the number of cells injected was 1×10^4 cells/mouse. For all other models, the number of cells injected was 2×10^5 cells/mouse. n=5 mice per model, except for PCNS#15 (n=2). **D)** Progression-free survival (PFS) of PCNSL patients from which PDX models were derived. PFS data was not available for patient PCNS#14.

developed neurological symptoms within as few as 25 days post-injection, suggesting that these tumors were highly aggressive (Figure 2.2C). PDX tumor aggressiveness was broadly correlated with shorter progression-free survival (PFS) in PCNSL patients from which the models were derived (Figure 2.2D). This correlation could not be made for PCNS#14 because the corresponding patient did not have a reported PFS.

We next assessed the histology of the PDX tumors by CD20, Ki67, and hematoxylin & eosin (H&E) immunohistochemistry (IHC). PDX tumors were highly infiltrative as shown by the diffuse staining of CD20 across the entire brain parenchyma in almost all models (Figure 2.3A). CD20 is a marker of B cells, which are absent in the non-tumor bearing mouse brain. Additionally, PDX tumors were highly proliferative as indicated by Ki67 staining and quantified using the MIB-1 proliferation index (Figure 2.3B). By H&E, we observed that tumor cells had an angiocentric growth pattern that was reminiscent of human PCNSL tumors (Figure 2.3C). Hans classification using the BCL-6, CD10, and MUM-1 IHC markers indicated that each PDX tumor was categorized into the same DLBCL subtype as the original human tumor. All PDX tumors were the NGC subtype except for PCNS#14, which was the GCB subtype (Figure 2.3D).

To assess whether PDX models remained genomically faithful to the human tumors, we examined both copy number and mutation profile. To assess copy number variations (CNV), we performed array comparative genomic hybridization (aCGH) in PCNSL patient tumors and early passage PDX tumors. Indeed, the CNVs of PDX models were similar to that of the respective patients
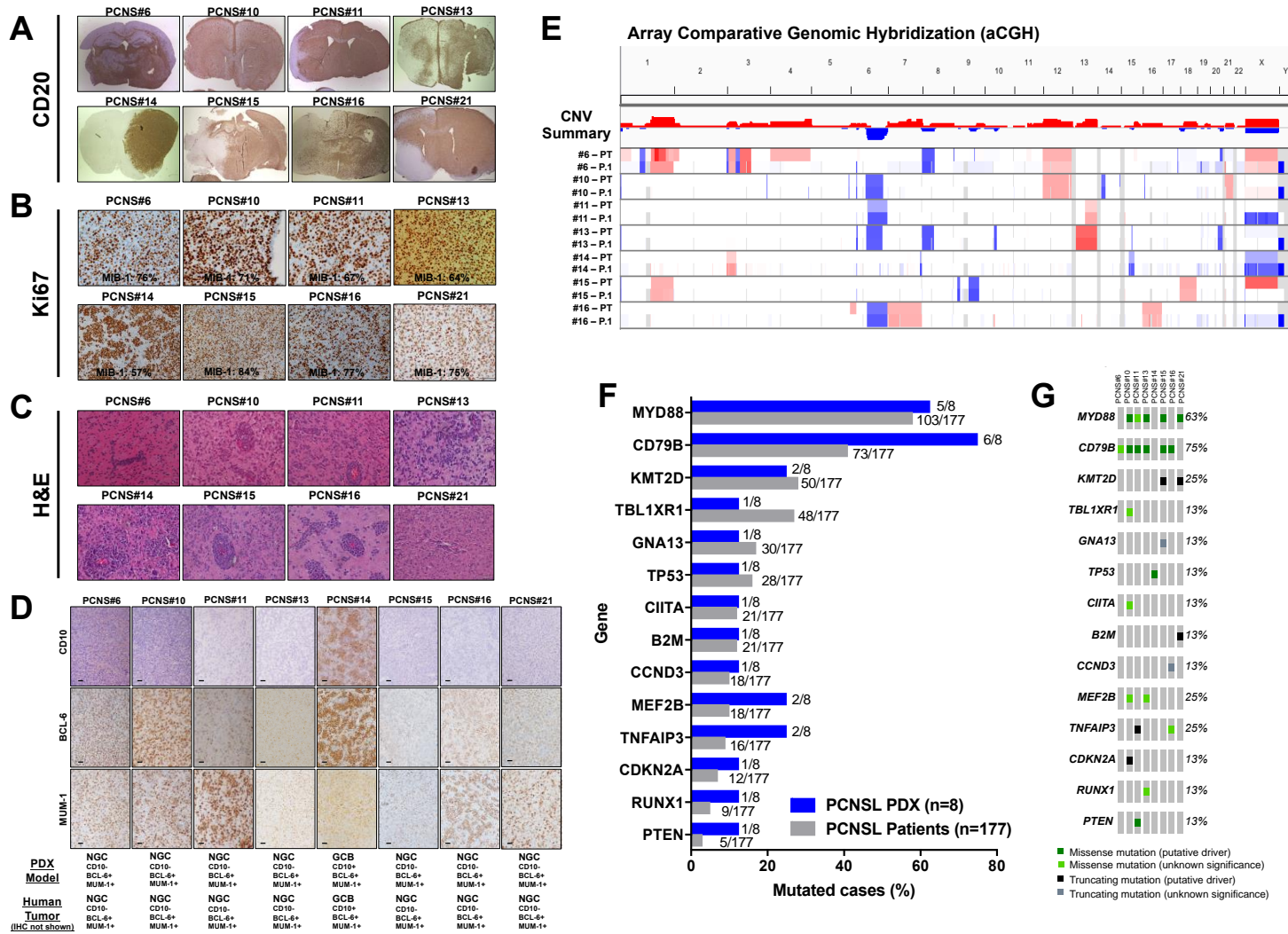
(Figure 2.3 description is continued on the next page)

Figure 2.3 (continued)

Figure 2.3. PCNSL PDX intracranial tumors are representative of human PCNSL. A) Immunohistochemistry (IHC) staining for the CD20 B cell marker in mouse coronal brain sections. **B)** IHC staining for the Ki67 proliferation marker and quantification using the MIB-1 proliferation index. **C)** IHC staining for hematoxylin and eosin (H&E). **D)** IHC staining for the Hans classification markers: CD10 (top row), BCL-6 (middle row), and MUM-1 (bottom row) in PDX models. Each column indicates a different PDX model. The Hans classification subtypes of PDX models and original human tumors are written below the PDX model IHC images. The IHC images for the original human tumors are not shown. NGC: Non-germinal center DLBCL, GCB: Germinal center B cell DLBCL. **E)** Array comparative genomic hybridization (aCGH) of patient and PDX at passage 1. Shades of red depict chromosome gains, and shades of blue depict chromosome losses. **F)** Frequency of genetic mutations in PDX models (n=8) and human PCNSL tumors (n=177). Genes are sorted by highest (top) to lowest (bottom) frequency of mutations found in human PCNSL tumors. **G)** Oncoprint of genetic mutations found in each PDX model.

(Figure 2.3E). Moreover, loss of chromosome 6q is often observed in human PCNSL (B. Chapuy et al., 2016) and is also detected in several of our PDX models, suggesting that our models are representative of this disease. We also performed targeted DNA sequencing of PDX tumors using the in-house MSKCC integrated mutation profiling of actionable cancer targets implicated in hematological malignancies (HemePACT), a panel of 576 genes. We found that the mutation frequencies of the most commonly altered genes in a previously sequenced cohort of 177 human PCNSL tumors were similar in our PDX tumors (Figure 2.3F). MYD88 and CD79B were the two most commonly mutated genes in both human PCNSL tumors and PDX tumors. Additionally, 50% (4/8) of PDX models had mutations in both MYD88 and CD79B (Figure 2.3G). These findings collectively demonstrated that our newly derived PDX models were representative of human PCNSL tumors with respect to growth in the CNS, tumor aggressiveness, histological features, and DNA copy number and mutation profiling.

We first evaluated whether the PDX models were biologically responsive to ibrutinib. We treated intracranial tumor-bearing mice with ibrutinib at 50 mg/kg daily by oral gavage, starting 5 days post-injection, and tracked mouse survival. A dose of 50 mg/kg is a standard dose and is similar to the dose used in other studies of ibrutinib in mice (Pouzoulet et al., 2019). We observed that ibrutinib did not prolong PCNS#11 mouse survival beyond a few days, if any, and we did not determine this result to be biologically meaningful (Figure 2.4A).

A PCNS#11 (intracranial, *in vivo*)
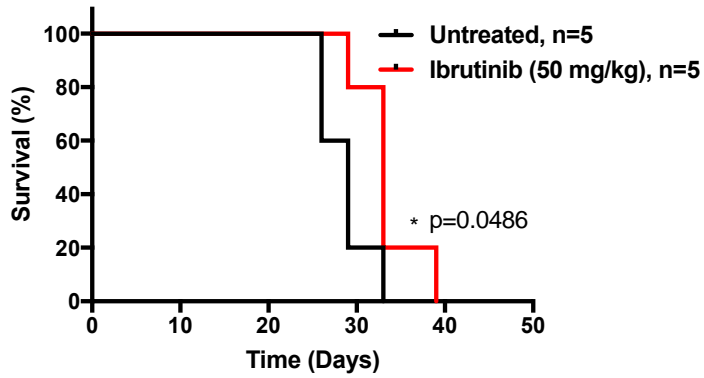
B PCNS#11 (subcutaneous, *in vivo*)

C PCNS#11 (cell line, *in vitro*)

D Inject 18 mice with PCNS#11 cell line (IC+SC)

22 days

Treat mice for 2 h
Vehicle, n=9
Ibrutinib, n=9

Collect for PK studies:
Plasma
IC tumor
SC tumor
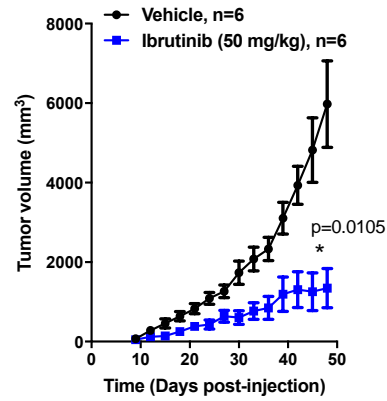
E PCNS#11 cell line PDX
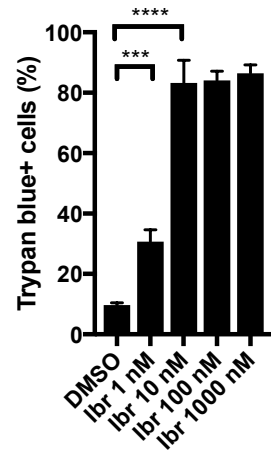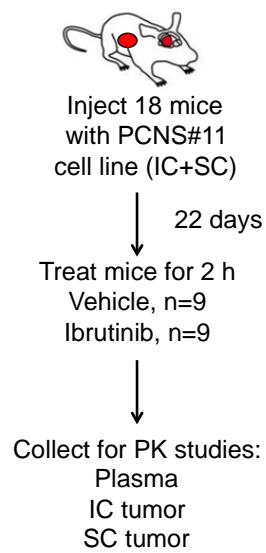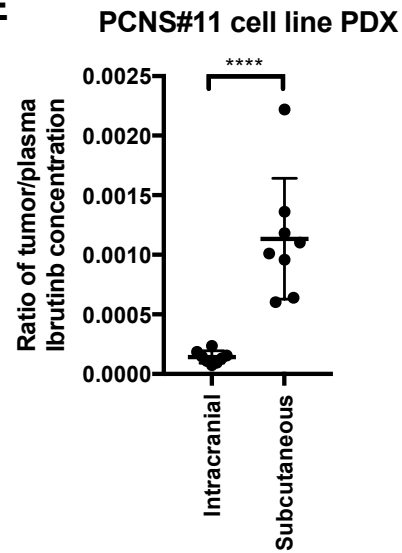
(Figure 2.4 description is continued on the next page)

Figure 2.4. Poor penetration of ibrutinib into the mouse CNS precludes *in vivo* study of ibrutinib response. A) Survival of mice bearing intracranial PCNS#11 PDX tumors treated with ibrutinib at 50 mg/kg daily by oral gavage. n=5 mice per group. Statistical significance was determined using the log-rank (Mantel-Cox) test: p=0.0486. **B)** Tumor volumes of mice bearing subcutaneous PCNS#11 PDX tumors treated with ibrutinib at 50 mg/kg daily by oral gavage. n=6 mice per group. Statistical significance was determined using an unpaired, parametric t-test: p=0.0105 (two-tailed). **C)** Cell viability of PCNS#11 cell line treated with ibrutinib dose titration for 4 days *in vitro*. Cell viability was assessed by Trypan blue dye exclusion. n=3 technical replicates. Statistical significance was determined using an unpaired, parametric t-test: DMSO vs. Ibr 1 nM, p=0.0008 (two-tailed); DMSO vs. Ibr 10 nM, p<0.0001 (two-tailed). **D)** Workflow for pharmacokinetic (PK) follow-up study using the PCNS#11 cell line injected into mice at both intracranial (IC) and subcutaneous (SC) sites. Mice were treated with vehicle or ibrutinib at 50 mg/kg for 2 h, and mouse plasma, IC tumor, and SC tumor were collected for analysis. **E)** Ratio of tumor (intracranial or subcutaneous) to plasma ibrutinib concentration in mice treated with ibrutinib at 50 mg/kg for 2 h. n=9 mice per group. Statistical significance was determined using an unpaired, parametric t-test: p<0.0001 (two-tailed).

However, we found that ibrutinib did slow the growth of PCNS#11 subcutaneous tumors *in vivo* (Figure 2.4B) and induced cell death in the PCNS#11 cell line *in vitro* (Figure 2.4C). To determine whether the discrepancy in ibrutinib response between intracranial and subcutaneous tumors was due to the pharmacokinetics (PK) of ibrutinib in mice, we performed a follow-up experiment where we measured the tumor and plasma ibrutinib concentration in mice bearing both intracranial and subcutaneous tumors (Figure 2.4D). We found that the ibrutinib concentration was nearly 10-fold lower in the intracranial compared to subcutaneous tumors, suggesting that the poor response in intracranial tumors may be attributed to the lower concentration of ibrutinib reaching the brain (Figure 2.4E).

Considering these limitations *in vivo*, we instead turned to an *ex vivo* tissue slice culture assay to evaluate the biological effect of ibrutinib in the PDX models. This *ex vivo* assay allowed us to use the desired concentration of ibrutinib and easily collect tissue for downstream protein and RNA analyses (Figure 2.5A). Since previous studies have reported that *ex vivo* culture may potentially alter PDX tumor cells, we performed RNA-seq on *ex vivo*-cultured ("*ex vivo*") and non-cultured ("*in vivo*") tumors to evaluate any differences in the transcriptomes. Based on unsupervised hierarchical clustering, we found that the "*ex vivo*" and "*in vivo*" samples still clustered together by PDX model, suggesting that *ex vivo* culture did not drastically alter the transcriptomes (Figure 2.5B). To

27
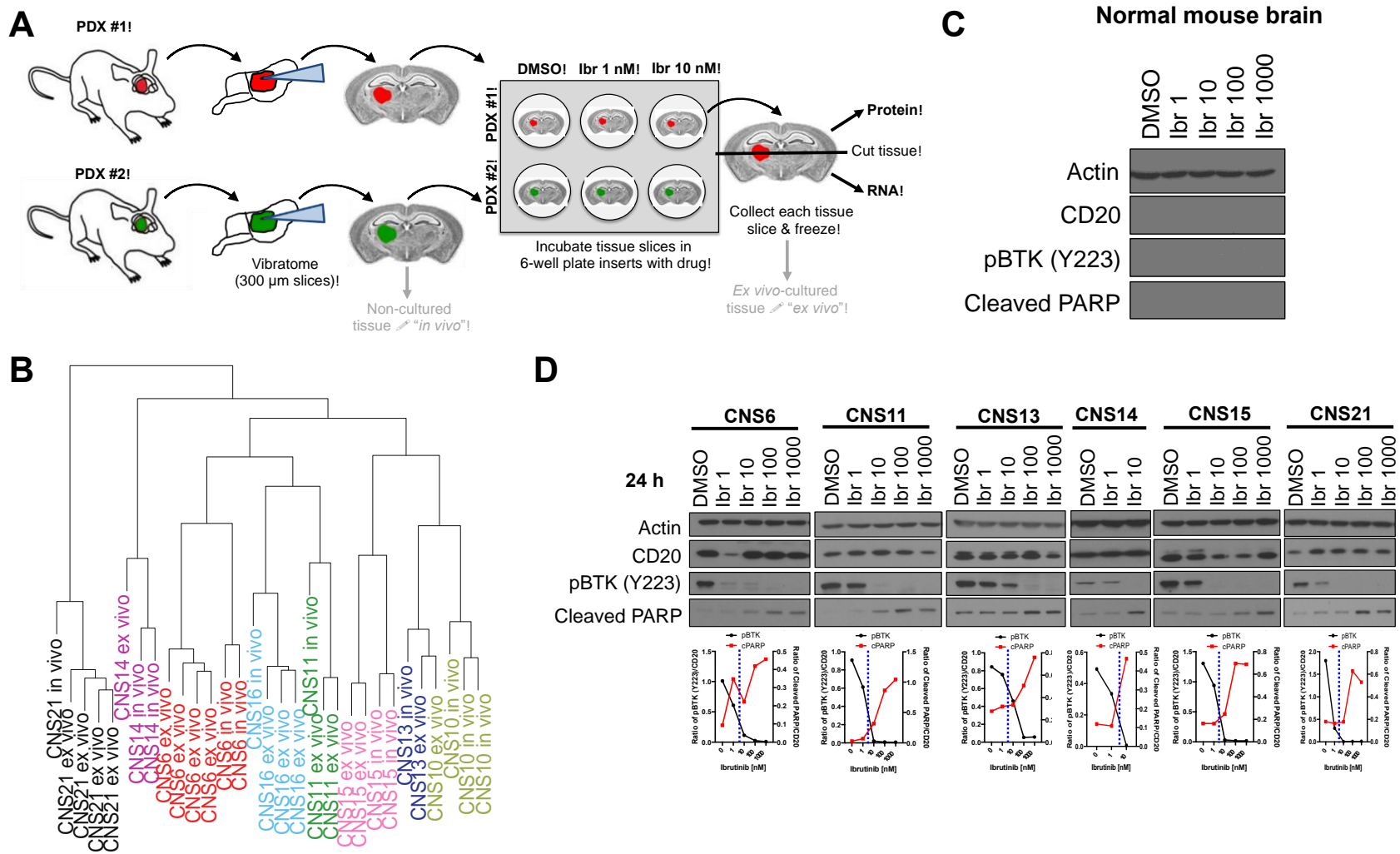
(Figure 2.5 description is continued on the next page)

Figure 2.5. Ibrutinib inhibits BTK and induces cell death in PDX models *ex vivo*. A) Workflow for *ex vivo* tissue slice culture assay. **B)** Hierarchical cluster dendrogram of RNA-seq samples of *ex vivo*-cultured PDX tumors (labeled "*ex vivo*") and non-cultured PDX tumors (labeled "*in vivo*") using the complete clustering method. PDX models are color-coded. **C)** Western blot of normal mouse brain treated *ex vivo* with ibrutinib. Ibrutinib concentrations are in nM. **D)** Western blots of PDX models treated *ex vivo* with ibrutinib for 24 h. Ibrutinib concentrations are in nM. Shown below each Western blot are the quantifications of pBTK (Y223) relative to CD20 (black line) and cleaved PARP relative to CD20 (red line). The dashed blue vertical line indicates the mean ibrutinib concentration (4.4 nM) detected in the CSF of PCNSL patients after 2 h treatment with 840 mg of ibrutinib.

A

	CNS6	CNS6	CNS11	CNS13	CNS14	CNS16	CNS21	CNS21

12 h   DMSO / Ibr 10 (for each pair)

pBTK (Y223)

CD20
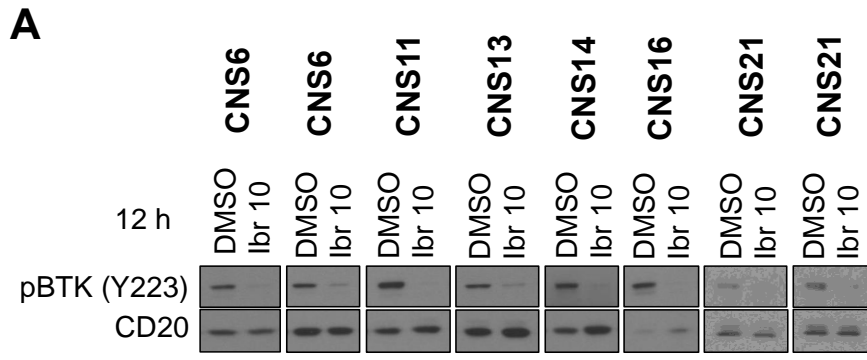
B

RNA-sequencing
PCNSL PDX models
(Ibrutinib 10 nM, DMSO)

↓

Differential gene expression
Ibrutinib 10 nM (n=10) vs.
DMSO (n=10)

↓

GSEA gene sets
Hallmark, n=50
C2 curated, n=6290

↓

129 gene sets down-regulated
by ibrutinib (FDR<0.05)

C

☐ GSEA Hallmark   ☐ NF-κB/TNFα signaling
☐ GSEA C2 Curated   ☐ Protein translation

MSigDB Collection	GSEA Gene set	PCNSL PDX models		
		NES Rank (n=129)	NES	FDR
Hallmark	HALLMARK_MYC_TARGETS_V2	1	-2.536	0.000
C2 Curated	REACTOME_RRNA_PROCESSING	2	-2.456	0.000
C2 Curated	SCHUHMACHER_MYC_TARGETS_UP	3	-2.444	0.000
C2 Curated	REACTOME_RRNA_MODIFICATION_IN_THE_NUCLEUS_AND_CYTOSOL	6	-2.273	0.000
C2 Curated	DANG_MYC_TARGETS_UP	7	-2.242	0.000
C2 Curated	BILD_MYC_ONCOGENIC_SIGNATURE	8	-2.217	0.000
Hallmark	HALLMARK_MYC_TARGETS_V1	11	-2.150	0.000
C2 Curated	SANSOM_APC_TARGETS_REQUIRE_MYC	13	-2.125	0.001
C2 Curated	KEGG_RNA_POLYMERASE	21	-2.022	0.003
C2 Curated	KEGG_RIBOSOME	26	-2.006	0.003
C2 Curated	SCHLOSSER_MYC_TARGETS_AND_SERUM_RESPONSE_DN	27	-2.003	0.003
C2 Curated	REACTOME_TRANSLATION	28	-2.001	0.003
C2 Curated	ZHOU_TNF_SIGNALING_30MIN	94	-1.792	0.026
Hallmark	HALLMARK_TNFA_SIGNALING_VIA_NFKB	129	-1.528	0.028

(Figure 2.6 description is continued on the next page)

(Figure 2.6 continued)

Figure 2.6. Protein translation and NF-κB/TNFα pathways are inhibited by ibrutinib in PCNSL PDX models. A) Western blots of PDX models treated *ex vivo* with DMSO or ibrutinib 10 nM for 12 h. Biological replicates: n=2 for CNS6 and CNS21, n=1 for all other models. **B)** RNA-seq analysis workflow. RNA-seq was performed on PDX models treated *ex vivo* with ibrutinib 10 nM or DMSO for 12 h. Biological replicates: n=2 for CNS6 and CNS21, n=1 for all other models. Technical replicates: n=2 for CNS21 samples, n=1 for all other samples. Differential gene expression analysis was performed using DESeq2 comparing all ibrutinib 10 nM vs. all DMSO-treated samples. n=10 samples per condition. All differentially expressed genes were ranked by log2 fold change and analyzed by GSEA Pre-ranked for Hallmark (n=50) and C2 curated (n=6290) gene sets. A total of 129 gene sets were significantly down-regulated by ibrutinib. Statistical significance was determined by multiple hypothesis testing using the GSEA method (Subramanian et al., 2005). A false discovery rate q-value (FDR) of less than 0.05 was considered to be significant. **C)** NF-κB/TNFα and protein translation gene sets decreased by ibrutinib in PDX models (FDR<0.05). Gene sets were ranked by the normalized enrichment score (NES). The NES and FDR for each gene set are shown in the table.

ensure that the signals we detected by Western blot were specific to human PCNSL tumor cells and not normal mouse brain cells, we performed an ibrutinib dose titration using normal mouse brain tissue *ex vivo* and did not detect any CD20, BTK, or cleaved poly ADP-ribose polymerase (PARP), a marker of apoptosis (Figure 2.5C). We next treated PDX models *ex vivo* with ibrutinib for 24 h and assessed BTK phosphorylation and PARP cleavage. We found that ibrutinib dose-dependently inhibited BTK phosphorylation and induced cleaved PARP, indicating apoptosis (Figure 2.5D). These results suggested that our PDX models were sensitive to ibrutinib *ex vivo*.

To determine the transcriptional effects of ibrutinib, we treated PDX models *ex vivo* with DMSO or ibrutinib 10 nM for 12 h. We confirmed that ibrutinib inhibited BTK phosphorylation in each PDX model experiment before performing RNA-seq (Figure 2.6A). For our RNA-seq data analysis, we grouped all ibrutinib-treated samples and all DMSO-treated samples for differential gene expression analysis. We then ranked all differentially expressed genes based on log2 fold change (log2fc) and ran gene set enrichment analysis (GSEA) with the Molecular Signatures Databases (MSigDB) Hallmark and C2 curated gene sets (Figure 2.6B). Based on GSEA, we found that ibrutinib significantly down-regulated 129 gene sets in PCNSL PDX models, which included many gene sets related to Myc, protein translation, and NF-κB/TNFα (Figure 2.6C).

Ibrutinib is fairly specific for BTK, but does inhibit other kinases with a C481 aligned with that of BTK. These kinases include B lymphoid tyrosine kinase (BLK), bone marrow tyrosine kinase gene on chromosome X (BMX), EGFR,

human epidermal growth factor receptor 2 (HER2), IL2 inducible T cell kinase (ITK), Janus kinase 3 (JAK3), and Tec protein tyrosine kinase (TEC) (Honigberg et al., 2010). To determine a BTK-specific response to ibrutinib, we utilized the PCNS#11 cell line (referred to as CNS11) to generate isogenic cell lines overexpressing empty vector (EV), BTK wild type (WT), or BTK C481S transgenes (Figure 2.7A). We confirmed that the cells expressing BTK C481S were fully resistant to ibrutinib (Figure 2.7B). We next performed RNA-seq followed by differential gene expression analysis for cell lines treated with ibrutinib 10 nM vs. DMSO for 12 h (Figure 2.7C). We found that many genes were significantly changed (FDR<0.05) by ibrutinib in EV clones, but not in BTK C481S clones. Any genes changed in BTK C481S clones were considered to be off-target effects of ibrutinib and were excluded. Of the genes that were left, 1002 genes were significantly changed in both EV clones. For each EV clone, these 1002 genes were ranked by log2fc to run GSEA for Hallmark and C2 curated gene sets (Figure 2.7C).

Based on GSEA, we observed that NF-κB/TNFα, Myc, and protein translation gene sets were also significantly down in the CNS11 EV clones. Moreover, there were 23 gene sets down that were shared between CNS11 EV clones and PCNSL PDX models, including 8 gene sets related to Myc/protein translation and 1 gene set related to NF-κB/TNFα (Figure 2.7D-E). This BTK-specific molecular response confirmed that the effects we observed in the PDX model *ex vivo* experiments were likely to be specific effects of BTK inhibition by ibrutinib.
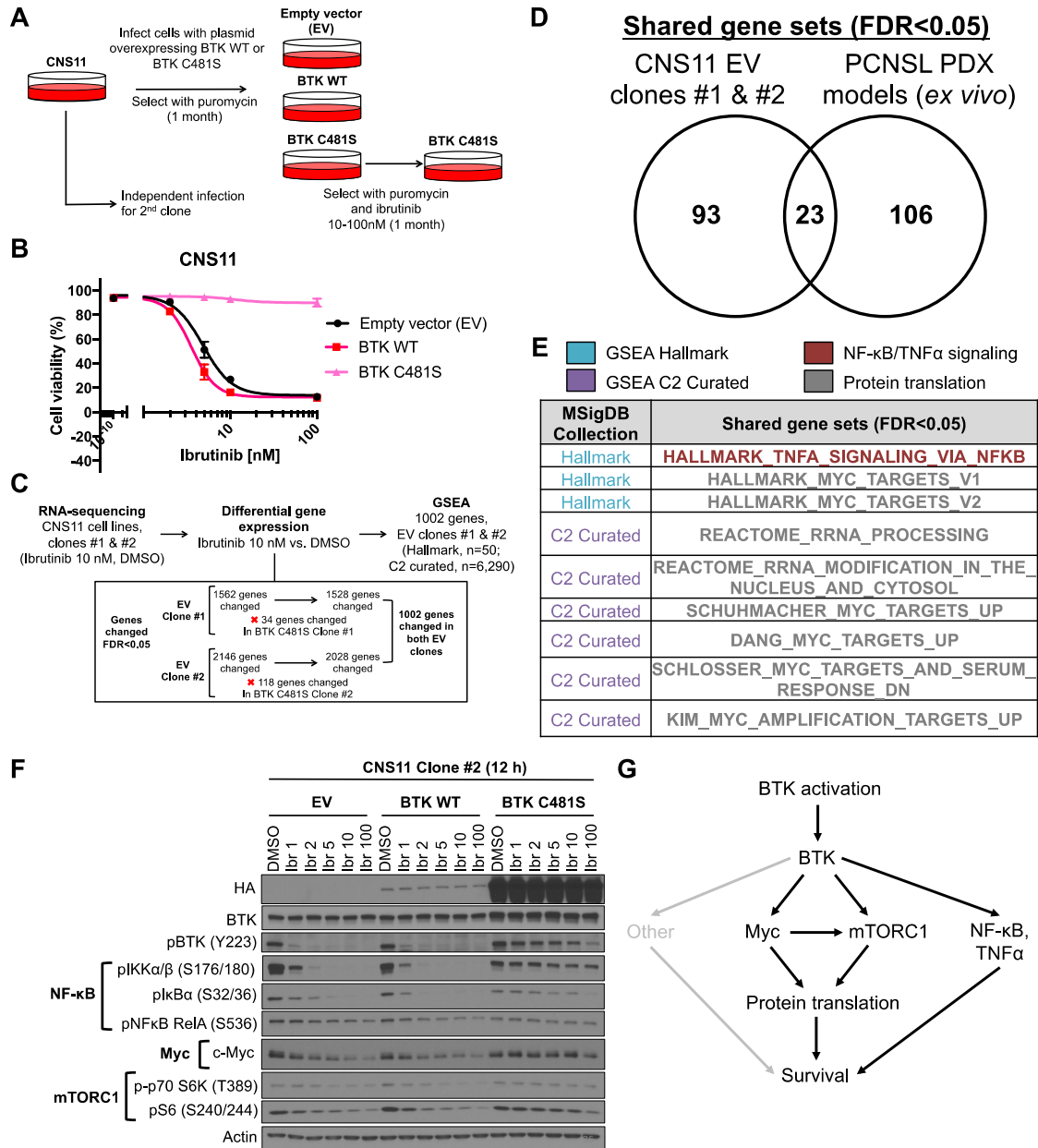
Figure 2.7. BTK regulates protein translation and NF-κB/TNFα in the PCNSL cell line. A) Derivation of PCNS#11 (CNS11) isogenic cell lines expressing empty vector (EV), BTK WT, or BTK C481S transgenes. All cells were selected with puromycin. Cells expressing BTK C481S were additionally selected with ibrutinib up to 100 nM. Two independent cell line clones were derived. **B)** Cell viability of CNS11 cell line clones treated with ibrutinib for 4 days. Cell viability was assessed by propidium iodide. n=2 biological replicates in independently

(Figure 2.7 continued)

derived clones. **C)** RNA-seq analysis workflow. RNA-seq was performed on CNS11 cell line clones #1 and #2 treated with ibrutinib 10 nM or DMSO for 12 h. n=2 technical replicates for each condition. Differential gene expression analysis was performed using DESeq2 comparing ibrutinib 10 nM vs. DMSO-treated samples. Any genes changed in BTK C481S-expressing clones were considered off-target and excluded from the list of genes changed in the respective EV clones. Genes that were decreased by ibrutinib in both EV clones (1002 genes) were ranked by log2 fold change and analyzed by GSEA Pre-ranked for Hallmark (n=50) and C2 curated (n=6290) gene sets. **D)** Venn diagram of GSEA gene sets significantly down-regulated by ibrutinib in CNS11 EV clones (116 gene sets total) and PCNSL PDX models (129 gene sets total). Statistical significance was determined by multiple hypothesis testing using the GSEA method (Subramanian et al., 2005). A false discovery rate q-value (FDR) of less than 0.05 was considered to be significant. **E)** NF-κB/TNFα and protein translation gene sets decreased by ibrutinib (FDR<0.05) in both CNS11 EV clones and PCNSL PDX models. Nine out of 23 total gene sets are shown in the table. **F)** Western blot of phospho-proteins in the BTK pathway through NF-κB, Myc, and mTORC1 in CNS11 Clone #2 treated with ibrutinib for 12 h. Ibrutinib concentrations are in nM. The exogenous BTK transgene is HA-tagged at the C-terminus. **G)** Model illustrating that BTK regulates NF-κB/TNFα and protein translation pathways through Myc and mTORC1 in PCNSL models.

Both Myc and mTORC1 are known to be master regulators of ribosome biogenesis and protein translation ("Correction for Pourdehnad et al., Myc and mTOR converge on a common node in protein synthesis control that confers synthetic lethality in Myc-driven cancers," 2013). To determine whether mTORC1 was also regulated downstream of BTK, we performed a Western blot with the CNS11 isogenic cell lines treated with an ibrutinib titration for 12 h. Indeed, we found that NF-κB and Myc, as well as mTORC1, were inhibited by ibrutinib in EV and BTK WT cells, but restored in the BTK C481S cells, suggesting that BTK regulated NF-κB, Myc, and mTORC1 axes in PCNSL (Figure 2.7F). Thus, we have evidence to support our model (Figure 2.7G) that NF-κB and protein translation pathways (Myc, mTORC1) are key mediators of signal transduction downstream of BTK specifically in PCNSL.

Conclusion:

In this chapter, we have defined the BTK-regulated transcriptome in PCNSL. We first established 8 novel PDX models of PCNSL that were representative of the human disease with respect to tumor aggressiveness, diffuse cell infiltration, high proliferation, and angiocentric growth in the mouse brain. We also demonstrated that the PDX models classified into the same DLBCL subtypes and shared similar genomic features, including CNV and genetic mutations, with human PCNSL tumors.

Using an *ex vivo* tissue slice culture assay, we showed that the PDX models were sensitive to ibrutinib as assessed by cleaved PARP. In these

ibrutinib-sensitive PDX models, we found that BTK inhibition led to significant down-regulation of gene expression related to NF-κB/TNFα signaling and protein translation, suggesting that these pathways were downstream of BTK. We also defined the BTK-specific effects of ibrutinib using CNS11 cells expressing the BTK C481S mutation, and found that similar genes involved in NF-κB/TNFα and protein translation were negatively changed by BTK inhibition with ibrutinib. NF-κB and TNFα are known to be activated by BTK signaling. However, BTK has not previously been reported to regulate protein translation (Myc, mTORC1) in PCNSL. Therefore, our work has identified novel effectors of the BTK pathway that may help promote the survival and pathogenesis of PCNSL tumors.

CHAPTER 3: MECHANISMS OF IBRUTINIB RESISTANCE
IN PCNSL

Introduction:

Despite the initial responses to ibrutinib in PCNSL patients, many patients eventually progressed, developing resistance to ibrutinib. The median PFS is 4.6 months in PCNSL patients, which is considerably shorter compared to that of patients with other B cell malignancies (Table 3.1). Following progression on ibrutinib, patients have few alternative therapy options and the prognosis is very poor. This indicates an urgent need to understand how resistance occurs and how to combat resistance in PCNSL.

The mechanisms of ibrutinib resistance have been reported in CLL, MCL, and WM patients with progressive disease, but have not been studied in PCNSL (Table 3.1). BTK mutations were detected in 61-67% of CLL patients (Maddocks et al., 2015; Woyach et al., 2017), but only in 16-20% of MCL and 16% of WM patients (Jain et al., 2018; Martin et al., 2016; L. Xu et al., 2017). Additionally, 6-15% of CLL patients had mutations in PLCG2 (Maddocks et al., 2015; Woyach et al., 2017). Co-occurrence of BTK and PLCG2 mutations were seen in 13-23% of CLL (Maddocks et al., 2015; Woyach et al., 2017), 16% of WM (L. Xu et al., 2017), and 1 MZL patient (Epperla et al., 2019). Moreover, CARD11 mutations were observed in MCL (5-8%) and WM (16%) patients, but not in CLL patients (Jain et al., 2018; Wu et al., 2016; L. Xu et al., 2017).

Disease	Median PFS (follow-up)	% BTK mutation	% PLCG2 mutation	% BTK & PLCG2 mutation	% CARD11 mutation	% BTK & CARD11 mutation	Reference
PCNSL	4.6 mo (15.9 mo)	?	?	?	?	?	Grommes et al., 2017
CLL	75%+ (26 mo)	61 - 67%	6 - 15%	13 - 23%			Byrd et al., 2013; Woyach et al., 2017; Maddocks et al., 2015
MCL	13.9 mo (15.3 mo)	16 - 20%			5 - 8%		Wang et al., 2013; Wu et al., 2016; Jain et al., 2018; Martin et al., 2016
WM	69%+ (24 mo)	16%		16%		16%	Treon et al., 2015; Xu et all., 2017

Table 3.1. Acquired ibrutinib resistance mutations in B cell malignancies. This table shows the median progression-free survival (PFS) of PCNSL, CLL, MCL, and WM patients on ibrutinib at the indicated follow-up time. The + symbol indicates the estimated PFS rate at the indicated follow-up time. The percentages of patients with BTK, PLCG2, BTK and PLCG2, CARD11, or BTK and CARD11 mutations are also shown. References are listed in the table and included in the reference list at the end of this dissertation (Byrd et al., 2013; Grommes et al., 2017; Jain et al., 2018; Maddocks et al., 2015; Martin et al., 2016; Treon et al., 2015; M. L. Wang et al., 2013; Woyach et al., 2017; Wu et al., 2016; L. Xu et al., 2017).

Mutations in BTK, PLCG2, and CARD11 have been characterized to some extent. The most common BTK mutation, C481S (or less frequently mutated to F, Y, or R), prevented the covalent binding of ibrutinib to BTK, rendering cells resistant to ibrutinib (Woyach et al., 2014). Other BTK mutations, such as T316A, T474I/S, or L528W, were also observed in patients who relapsed on ibrutinib (Maddocks et al., 2015; Sharma et al., 2016). The PLCG2 R665W and L845F mutations detected in CLL were shown to increase intracellular calcium flux and mediate downstream signaling independently of BTK, such as through AKT or extracellular signal-regulated kinase (ERK) (Woyach et al., 2014). Various CARD11 mutations have been identified as oncogenic or associated with primary or acquired ibrutinib resistance, and nearly all mutations occurred in the coiled-coil domain (Bartlett et al., 2018; Caeser et al., 2021; Chan, Schaffer, & Pomerantz, 2012; Dong et al., 2011; Fox et al., 2018; Lenz et al., 2008; Watt et al., 2015; Wu et al., 2016; L. Xu et al., 2017). CARD11 mutations block its auto-inhibition and therefore keep CARD11 in a constitutively active conformation (Lamason, McCully, Lew, & Pomerantz, 2010; Y.-K. Yang et al., 2016). In addition, many CARD11 mutations were shown to increase NF-κB activation (Chan et al., 2012; Dong et al., 2011; Lenz et al., 2008; Watt et al., 2015).

The resistance mechanisms to ibrutinib have not yet been reported in PCNSL. In this chapter, we identified candidate resistance mutations in PLCG2 and CARD11, but not BTK, in novel PCNSL cell line models of acquired resistance and PCNSL patients in our clinical study. We found that CARD11 mutations were associated with worse PFS in PCNSL patients on ibrutinib

therapy. Moreover, we demonstrated that specific CARD11 mutations restored MALT1 and mTOR activity, but that only ibrutinib combined with mTOR inhibitor effectively induced cell death in CARD11-mutant PCNSL cells. Thus, our findings have pointed to a potential strategy to overcome CARD11 mutation-mediated resistance to ibrutinib in PCNSL.

Results:

To study the mechanisms of acquired ibrutinib resistance in PCNSL, we first independently derived 3 ibrutinib-resistant sublines, which we called CNS11-RA, CNS11-RB, and CNS11-RC, by culturing the CNS11 cell line in increasing concentrations of ibrutinib up to 100 nM for 1-8 months (Figure 3.1A). All 3 sublines were fully resistant to ibrutinib (Figure 3.1B) and had fully or partially restored signaling through the BTK pathway, including NF-κB and mTOR (Figure 3.1C-D). CNS11-RA was the most biochemically resistant to ibrutinib. Targeted mutation profiling of the 3 sublines by MSKCC HemePACT revealed that each ibrutinib-resistant subline gained a different mutation in PLCG2 and the CNS11-RA subline acquired an additional CARD11 mutation (Figure 3.1E). PLCG2 R665L and E39K were identified in CNS11-RB and CNS11-RC, respectively. CNS11-RA acquired mutations in both PLCG2 L848P and CARD11 F130V. CNS11-RA also acquired missense mutations in PDS5 cohesin associated factor B (PDS5B) and roundabout guidance receptor 1 (ROBO1), which encode tumor suppressor proteins involved in sister chromatid adhesion and cell adhesion, respectively
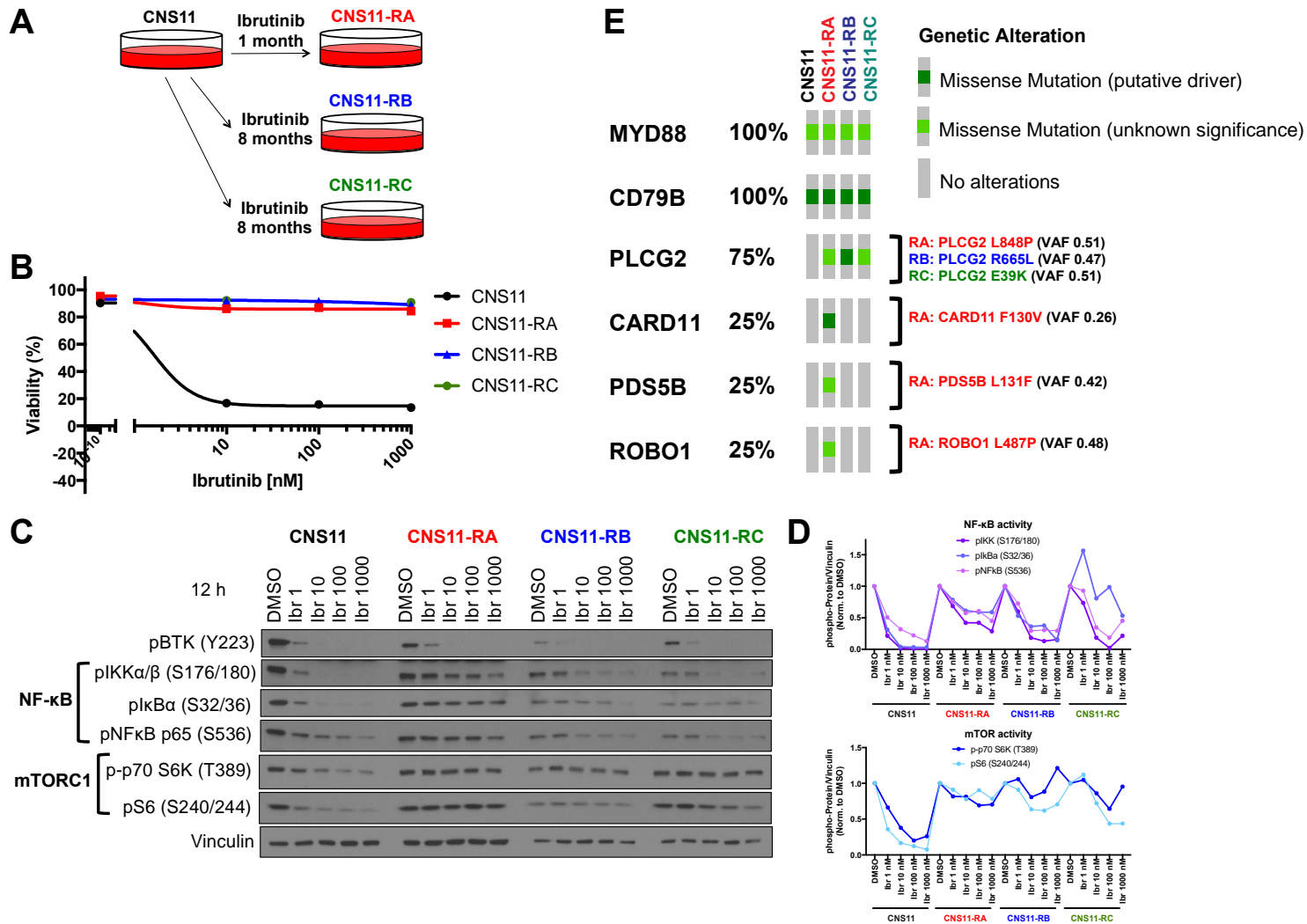
(Figure 3.1 description continued on the next page)

Figure 3.1. Identification of CARD11 and PLCG2 mutations in PCNSL cell lines with acquired resistance to ibrutinib. A) Independent derivation of 3 ibrutinib-resistant sublines by culturing the CNS11 ibrutinib-sensitive cell line in increasing concentrations of ibrutinib (1-100 nM) up to 8 months. **B)** Cell viability in CNS11 sublines treated with ibrutinib for 4 days. Cell viability was measured by Trypan blue dye exclusion. n=3 technical replicates. **C)** Western blot of the BTK pathway through NF-κB and mTORC1 in CNS11 sublines treated with ibrutinib for 12 h. Ibrutinib concentrations are in nM. **D)** Western blot quantification of NF-κB and mTORC1 activity using ImageJ software. The signal of each phospho-protein was normalized to that of vinculin, and then normalized to the DMSO sample of each subline. **E)** Targeted mutation profiling by MSKCC HemePACT in CNS11 sublines. The oncoprint shows the genes mutated within the BCR pathway (MYD88, CD79B) and genes with acquired mutation in at least one of the CNS11 sublines. CNS11 sublines are color-coded. Specific mutations and variant allele frequencies (VAF) for each gene are shown to the right of the oncoprint.
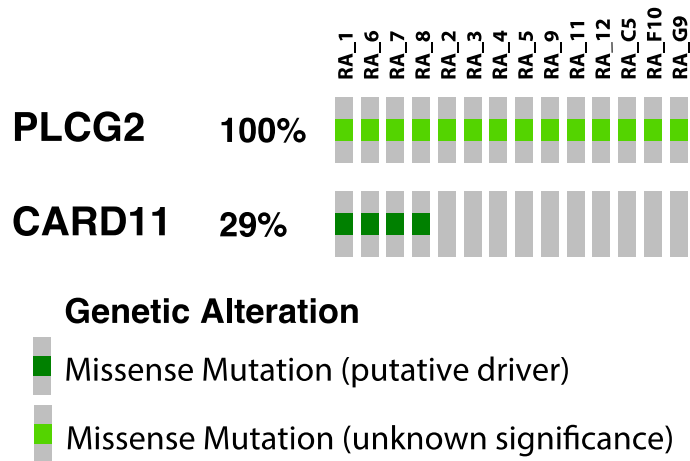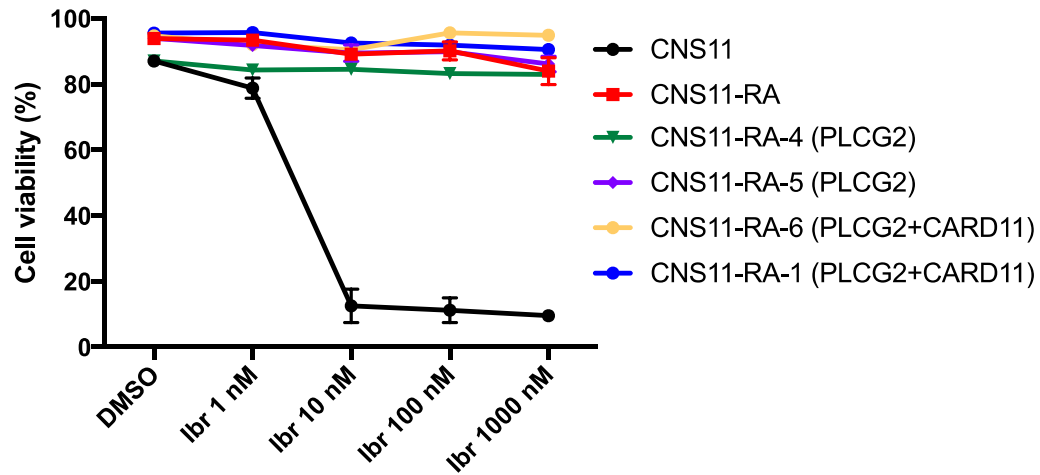
(Figure 3.2 description continued on the next page)

Figure 3.2. CARD11 and PLCG2 mutations are not mutually exclusive in the CNS11-RA cell line. A) Targeted mutation profiling by MSKCC HemePACT in CNS11-RA single cell clones. The oncoprint shows the status of PLCG2 and CARD11 mutations in each single cell clone. n=14 single cell clones. **B)** Cell viability in 2 CNS11-RA single cell clones with only PLCG2 mutation (CNS11RA-4, CNS11-RA-5) and 2 CNS11-RA single cell clones with both PLCG2 and CARD11 mutations (CNS11-RA-6, CNS11-RA-1). Cells were treated with ibrutinib for 4 days, and cell viability was assessed by Trypan blue dye exclusion. n=3 technical replicates.

(Denes, Pilichowska, Makarovskiy, Carpinito, & Geck, 2010; Jiang et al., 2019; Parray et al., 2014). Neither PDS5B nor ROBO1 mutations have been implicated in ibrutinib resistance, although ROBO1 expression and methylation have been investigated in MCL and CLL (Appe et al Int J Lab Hematol 2017). Curiously, we did not detect any BTK mutations in these ibrutinib-resistant sublines.

To determine whether the PLCG2 L848P and CARD11 F130V mutations identified in CNS11-RA were mutually exclusive, we performed single cell cloning and derived 14 single cell clones of CNS11-RA. We sequenced each clone by MSKCC HemePACT and found that all single cell clones had the PLCG2 mutation and 4/14 (29%) clones had both PLCG2 and CARD11 mutations, suggesting that these mutations were not mutually exclusive (Figure 3.2A). Moreover, the PLCG2 mutation was likely an earlier event since all cells had this mutation. Our preliminary cell viability data showed no differences in the biological resistance to ibrutinib in single cell clones with the PLCG2 mutation (CNS11-RA-4, CNS11-RA-5) vs. single cell clones with both PLCG2 and CARD11 mutations (CNS11-RA-6, CNS11-RA-1) (Figure 3.2B).

Since PLCG2 and CARD11 mutations were identified in our PCNSL cell lines and were reported in other B cell malignancies with ibrutinib resistance, we examined whether mutations in these genes also occurred in our PCNSL patients on ibrutinib therapy. We identified 2 PCNSL patients with PLCG2 mutations, 1 primary resistance mutation identified in the patient's tumor and 1 acquired resistance mutation identified in the patient's CSF (Figure 3.3A). We also had 5 patients with CARD11 mutations, all of which were primary resistance

mutations identified in the patients' tumors (Figure 3.3A). The magnetic resonance images (MRI) of Patient #1 with CARD11 R179Q at enrollment and at progression are shown (Figure 3.3B). Interestingly, we found that CARD11 mutation was associated with shorter PFS in PCNSL patients on ibrutinib, suggesting that CARD11 mutation may have a role in ibrutinib progression (Figure 3.3C). CARD11 mutation status did not correlate with shorter PFS in PCNSL patients treated with chemotherapy. Of note, we did not detect any BTK mutations in PCNSL patients in our ibrutinib study.

Out of the 5 total PLCG2 mutations we identified in either our PCNSL cell lines or PCNSL patients, 3 of these mutations, A420T, E39K, and R665L, was novel. The PLCG2 D1140N mutation was previously reported in CLL patients with acquired resistance to ibrutinib (Jones et al., 2017). The PLCG2 L848P mutation was found in a patient with autoinflammation, antibody deficiency, and immune dysregulation (APLAID), and this mutation was shown to be gain-of-function compared to PLCG2 WT (Neves et al., 2018). We also identified a total of 7 CARD11 mutations in our PCNSL studies. Three were novel CARD11 mutations: R179Q, R337Q, and S212N (Table 3.2). The other 4 CARD11 mutations we identified either in our PCNSL cell line or PCNSL patients were previously reported in other studies (Bartlett et al., 2018; Dong et al., 2011; Lenz et al., 2008; Wu et al., 2016).

Since we observed that CARD11 mutation status correlated with worse PFS in PCNSL patients on ibrutinib, we further characterized several of these CARD11 mutations, including F130V identified in the CNS11-RA cell line, and

A

CARD11 mutation
5/46 patients (10.8%)

PLCG2 mutation
2/46 patients (4.3%)

PCNSL Patient	Gene	Mutation	Mutation Type	Days to progression
1	CARD11	R179Q	Primary	58 days
2	CARD11	S212N	Primary	36 days
3	CARD11	L251P/D230N	Primary	7 days
4	CARD11	R337Q	Primary	179 days
5	CARD11	K215N	Primary	110 days
6	PLCG2	A420T	Primary	28 days
7	PLCG2	D1140N	Acquired	140 days

B

Patient #1: Primary resistance
CARD11 R179Q

Enrollment   58 days to progression
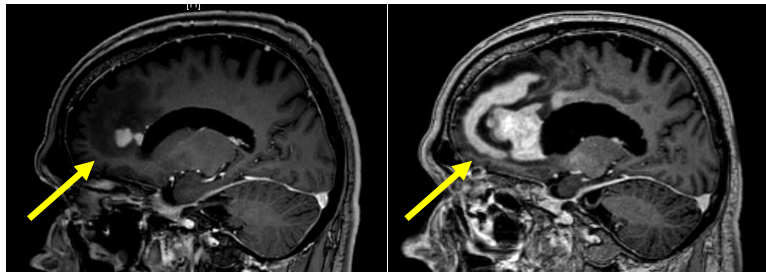
C **PFS based on CARD11 mutation status**

— CARD11 WT, n=41

--- CARD11 MUT, n=5

p=0.0128
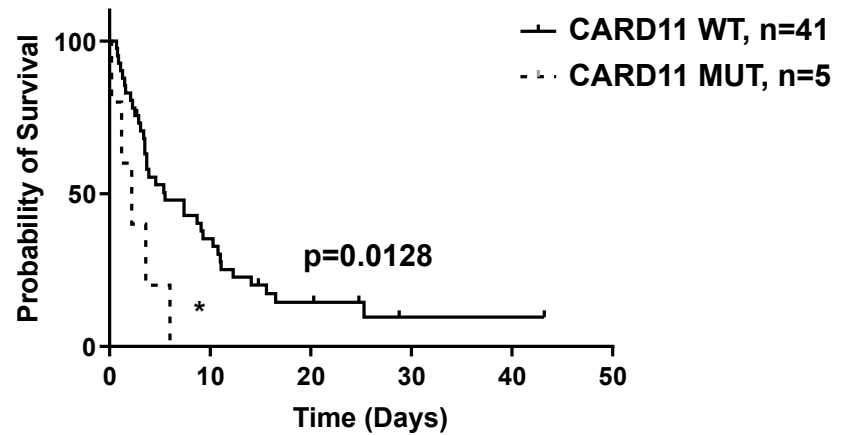
(Figure 3.3 description continued on the next page)

Figure 3.3. Identification of CARD11 and PLCG2 mutations in PCNSL patients on ibrutinib. A) Primary and acquired resistance mutations in CARD11 and PLCG2 identified in PCNSL patients who progressed on ibrutinib. Patient #3 had 2 different CARD11 mutations. **B)** MRI scans of Patient #1 with CARD11 R179Q mutation at enrollment and at progression. The yellow arrow indicates the site of the tumor within the brain. **C)** Progression-free survival (PFS) based on CARD11 mutation status of PCNSL patients on ibrutinib therapy. CARD11 WT, n=41 patients; CARD11 MUT, n=5 patients. Statistical significance was determined using the log-rank (Mantel-Cox) test: p=0.0128.

PCNSL Source	CARD11 Mutation	Mutation type	Is the CARD11 mutation novel?	Reference
Cell line	F130V	Acquired	No - DLBCL (oncogenic)	Dong et al., 2011
Patient	R179Q	Primary	Yes	
Patient	R337Q	Primary	Yes	
Patient	S212N	Primary	Yes	
Patient	L251P	Primary	No - DLBCL (oncogenic)	Lenz et al., 2008
Patient	K215N	Primary	No - MCL (resistance)	Wu et al., 2016
Patient	D230N	Primary	No - MCL (acquired resistance), FL (primary resistance), DLBCL (oncogenic)	Wu et al., 2016; Bartlett et al., 2018; Lenz et al., 2008

Table 3.2. CARD11 mutations identified in our PCNSL studies. Listed are the CARD11 mutations we found in either our PCNSL cell line or PCNSL patients treated with ibrutinib, including the type of mutation (primary or acquired) and whether the mutation is novel or has previously been reported in other B cell malignancies as an oncogenic, primary resistance, or acquired resistance mutation. References are listed in the table and included in the reference list at the end of this dissertation (Bartlett et al., 2018; Dong et al., 2011; Lenz et al., 2008; Wu et al., 2016). DLBCL: diffuse large B cell lymphoma, MCL: mantle cell lymphoma, FL: follicular lymphoma.

R179Q and R337Q, identified in PCNSL Patients #1 and #4, respectively. Using the CNS11 cell line, we generated isogenic cell lines expressing WT or mutant CARD11 (Figure 3.4A). All 3 CARD11 mutations conferred resistance to ibrutinib (Figure 3.4B). Overexpression of CARD11 WT also conferred resistance, although not as strongly as the mutants. To determine whether the BTK pathway was restored in CARD11-mutant cells, we performed a Western blot using cells treated with ibrutinib 5 or 10 nM for 12 h. We found that both CARD11 WT and CARD11-mutant cells had increased phosphorylation at CARD11 S652, indicating CARD11 activation (Figure 3.4C). However, only the CARD11-mutant cells had restored MALT1 proteolytic activity and mTOR activity, suggesting that these pathways may be mediating ibrutinib resistance (Figure 3.4C-E).

Both MALT1 and mTOR can be targeted with small molecule inhibitors. We first tested the MALT1 inhibitor, SCM-02-138 (SCM), and confirmed that MALT1 inhibition blocked the cleavage of its substrates, BCL10 and Roquin, in CNS11 parental cells (Figure 3.5A). We found that SCM combined with ibrutinib did not induce cell death in the CNS11 CARD11-mutant cells (Figure 3.5B). We next tested ibrutinib combined with the mTOR inhibitor rapamycin, and found that this combination strongly induced cell death (Figure 3.5C). Moreover, BTK and mTORC1 were effectively inhibited in CNS11 CARD11-mutant cells treated with ibrutinib and rapamycin (Figure 3.5D). Our results suggested that ibrutinib combined with rapamycin might be a potential strategy to overcome CARD11 mutation-mediated ibrutinib resistance in PCNSL.

A Generate isogenic cell lines overexpressing CARD11 WT or mutants (MUT)

CNS11

Select with puromycin (1 month)

Empty vector (EV)

CARD11 WT

CARD11 MUT

B

Cell viability (%)

EV | CARD11 WT | CARD11 F130V | CARD11 R179Q | CARD11 R337Q

C CNS11 (12 h)

CARD11

EV | WT | F130V | R179Q | R337Q

pBTK (Y223)
HA
CARD11
pCARD11 (S652)

mTORC1 [pPRAS40 (T246) / pS6 (S240/244)]

MALT1 [Roquin (cleaved) / Bcl10 (uncleaved)]

Cleaved caspase 3
Actin

D mTORC1 activity
pPRAS40 (T246)
pS6 (S240/244)

phospho-Protein/Actin (Norm. to DMSO)

EV | CARD11 WT | CARD11 F130V | CARD11 R179Q | CARD11 R337Q

MALT1 activity
Roquin (cleaved)
BCL10 (uncleaved)

phospho-Protein/Actin (Norm. to DMSO)

EV | CARD11 WT | CARD11 F130V | CARD11 R179Q | CARD11 R337Q

E

BTK activation

BTK → PLCG2

Other | Myc → mTORC1 ← CARD11

MALT1 cleave

Protein translation | BCL10, Roquin, others

Survival | NF-κB, TNFα | Other

(Figure 3.4 description is continued on the next page)

Figure 3.4. CARD11 mutations restore MALT1 and mTOR activity in PCNSL. A) Generation of isogenic CNS11 cell lines expressing CARD11 wild type (WT) or mutant (MUT) transgenes. **B)** Cell viability in CNS11 cell lines treated with ibrutinib for 4 days. Cell viability was assessed by propidium iodide. n=2 biological replicates. Statistical significance was determined using an unpaired, parametric t-test: * indicates $p<0.05$ (two-tailed), ** indicates $p<0.005$ (two-tailed), ns=not significant. **C)** Western blot of the BTK pathway through mTORC1 and MALT1 in CNS11 cell lines treated with ibrutinib for 12 h. Ibrutinib concentrations are in nM. The CARD11 transgene is HA-tagged at the C-terminus. **D)** Western blot quantification of mTORC1 and MALT1 activity using ImageJ software. The signal of each phospho-protein was normalized to that of actin, and then normalized to the DMSO sample of EV cells. **E)** Model for CARD11 mutation-mediated restoration of mTORC1 and MALT1 activity in PCNSL cells.

A

CNS11

BCL10 (uncleaved)

Roquin (cleaved)

Actin

B

Ibrutinib + SCM-02-138

C

Ibrutinib + Rapamycin (n=3)

D

CNS11 (12 h)
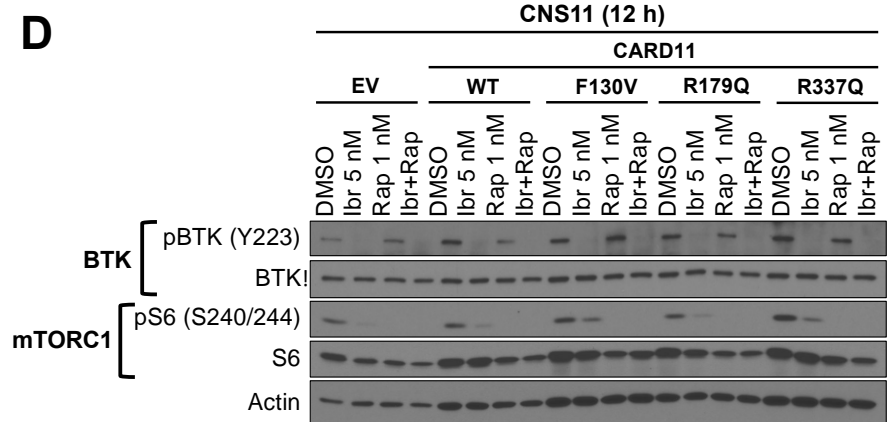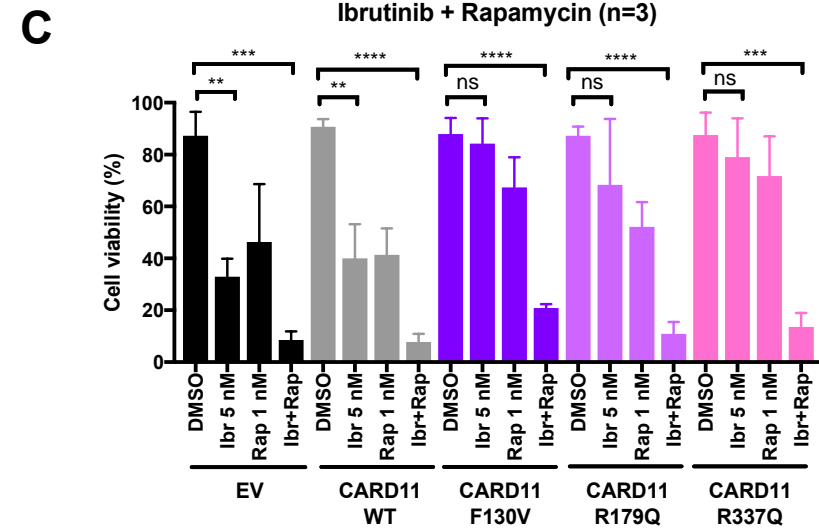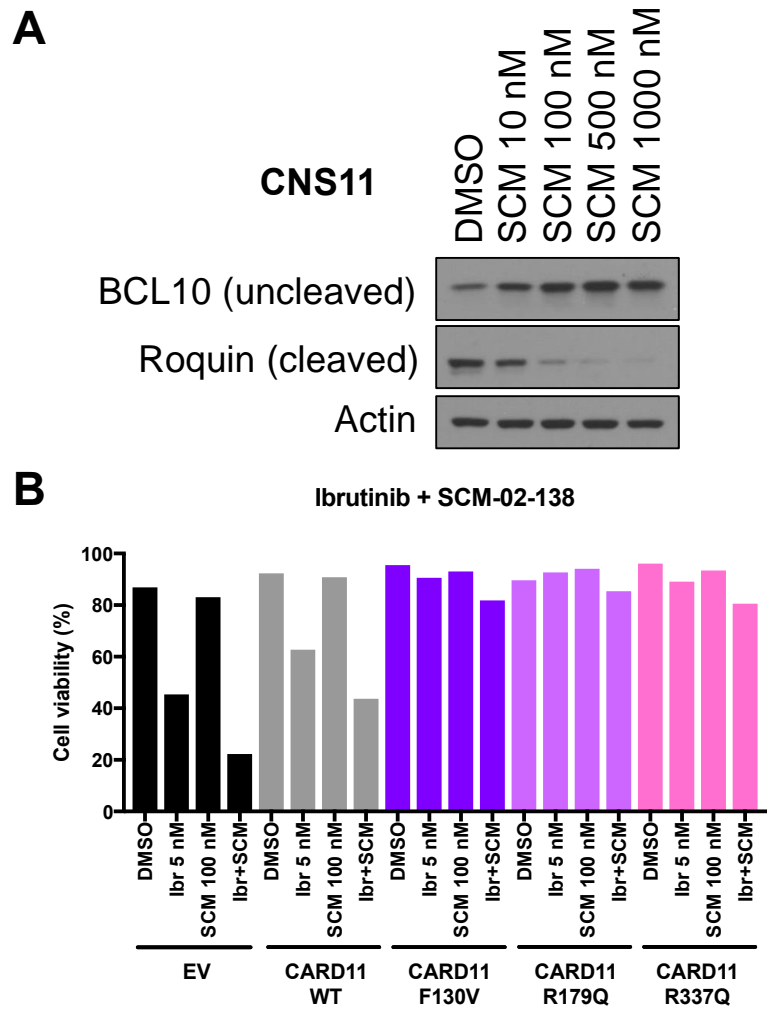
(Figure 3.5 description is continued on the next page)

54

Figure 3.5. mTOR inhibitor, but not MALT1 inhibitor, sensitizes CARD11-mutant cells to ibrutinib. A) Western blot of the MALT1 substrates, BCL10 and Roquin, in the CNS11 parental cell line treated with the MALT1 inhibitor SCM-02-138 (SCM) for 24 h. **B)** Cell viability in CNS11 isogenic cell lines treated for 4 days with ibrutinib (5 nM), SCM (100 nM), or the combination. Cell viability was assessed by propidium iodide. n=1 sample per condition. **C)** Cell viability in CNS11 isogenic cell lines treated for 4 days with ibrutinib (5 nM), rapamycin (1 nM), or the combination. Cell viability was assessed by propidium iodide. n=3 biological replicates. Statistical significance was determined using an unpaired, parametric t-test: ** indicates p<0.005 (two-tailed), *** indicates p<0.0005 (two-tailed), **** indicates p<0.0001 (two-tailed), ns=not significant. **D)** Western blot of BTK and mTORC1 activity in CNS11 isogenic cell lines treated with ibrutinib, rapamycin, or the combination for 12 h.

Conclusion:

In this chapter, we identified candidate resistance mutations in CARD11 and PLCG2, but not BTK, in our PCNSL cell lines and PCNSL patients on ibrutinib therapy. In addition, we detected point mutations in PDS5B and ROBO1 in the CNS11-RA cell line with acquired resistance. Both of these genes encode tumor suppressor proteins, and have not previously been described in the context of ibrutinib resistance.

CARD11 mutation in particular was associated with shorter PFS in PCNSL patients, indicating a critical role for CARD11 in mediating resistance to ibrutinib. We investigated specific mutations in CARD11 F130V, R179Q, and R337Q, and found that PCNSL cells expressing these mutations restored MALT1 and mTOR activity. Moreover, ibrutinib combined with mTOR inhibitor, but not MALT1 inhibitor, overcame resistance in CARD11-mutant PCNSL cells.

In summary, we have found CARD11 and PLCG2 mutations as mechanisms of resistance to ibrutinib in PCNSL cell lines and patients. Moreover, we investigated ibrutinib-based combination therapies to combat CARD11 mutation-mediated resistance.

CHAPTER 4: DISCUSSION AND FUTURE DIRECTIONS

Development of PCNSL PDX models that share key features of human PCNSL

PCNSL is a rare, aggressive primary brain tumor with poor prognosis. The derivation of laboratory models is critical to help us further understand the disease in order to improve patient outcomes. We have developed 8 novel PCNSL PDX models and rigorously shown that the models were histologically and genetically faithful to the human disease with respect to CNS tropism, tumor aggressiveness, diffuse infiltration and proliferation, angiocentric growth, Hans subtype, and DNA copy number and mutation profile. Two studies have previously reported the development and characterization of PCNSL PDX models (Pouzoulet et al., 2019; Tateishi et al., 2020). Our work is unique in that we utilized our PDX models in *ex vivo* tissue slice culture assays to evaluate the biological and transcriptional effects of ibrutinib in order to uncover novel pathways that may be important for the biology and pathogenesis of PCNSL.

A future direction would be to investigate how the PDX models might change over serial passage in mice. Previous studies in BCR-ABL1 lymphoblastic leukemia have demonstrated that dominant clones may either persist or be outcompeted by subclonal populations over time (Notta et al., 2011). We have preliminary data in our PDX models to suggest that the histological features, subtype classification, and genetics are relatively stable

over serial passage. However, further analysis will be needed to investigate whether specific clonal or subclonal populations shift over serial passage.

Molecular response to ibrutinib in PCNSL models

In our PDX models, which we demonstrated to be sensitive to ibrutinib, we found that ibrutinib treatment reduced the expression of genes related to NF-κB/TNFα and protein translation, including prominent down-regulation of Myc target genes. We also derived a BTK-specific ibrutinib response signature in our PCNSL cell line by using the BTK C481S mutation to identify and exclude off-target effects of ibrutinib. We saw similar enrichment of NF-κB/TNFα and protein translation genes that were decreased by ibrutinib, further indicating that these pathways were regulated downstream of BTK in PCNSL. Both Myc and mTOR are known to control ribosome biogenesis and protein translation (Chauvin et al., 2014; Holz et al., 2005; Mamane et al., 2006; Schmidt, 2004). Myc is a transcription factor that promotes expression of many ribosome genes and translation initiation factors. mTOR, specifically mTORC1, is a protein kinase that phosphorylates 4E-BP1 and S6K to promote protein translation. Myc and mTORC1 also converge in their regulation of protein translation, cell growth, and survival. Previous studies have found that mTORC1, and particularly phosphorylation of 4E-BP1, is critical for Myc-mediated tumorigenesis ("Correction for Pourdehnad et al., Myc and mTOR converge on a common node in protein synthesis control that confers synthetic lethality in Myc-driven cancers," 2013; Liu et al., 2017). Myc has also been found to inhibit TSC2, a tumor

suppressor and negative regulator of mTORC1, thereby activating mTORC1 (Ravitz, Chen, Lynch, & Schmidt, 2007). Moreover, S6K has been reported to mediate the translation of Myc mRNA (Csibi et al., 2014; Wall et al., 2008). Our transcriptional and biochemical data have indicated that BTK regulated protein translation through both Myc and mTORC1 in PCNSL.

These findings have not previously been reported in PCNSL. However, BTK is known to activate NF-κB and TNF expression (Page et al., 2018), and both BCR/PI3K/AKT and CD40/NF-κB signaling pathways promote the expression of Myc and phosphorylation of S6, a downstream effector of mTORC1, in GC B cells (Luo, Weisel, & Shlomchik, 2018). Moreover, Myc protein was decreased in DLBCL cells treated with AKT inhibitor, suggesting that Myc was regulated downstream of AKT (Erdmann et al., 2017). Myc expression through CD40/NF-κB was also shown to rescue B cell lymphoma cells from apoptosis induced by IgM (Schauer, Wang, Sonenshein, & Rothstein, 1996). We do not know whether Myc is critical for PCNSL survival and pathogenesis. However, since Myc is important for the biology of B cells and B cell lymphomas, it would not be surprising if this were also true for PCNSL.

Myc expression/rearrangement or mTOR activity has been evaluated in PCNSL to identify prognostic markers. One study assessed mTOR activity by IHC on PCNSL cases for p-4E-BP1 (T37/46), p-S6 (S235/236), and Ras homolog enriched in brain (Rheb), and found that all 24 cases examined had positive expression of at least 1 of these markers, and 12/24 (50%) had positive expression of all 3 markers, indicating that mTORC1 was active in these PCNSL

tumors (Nitta, Nakasu, Shima, & Nozaki, 2016). The mTOR inhibitor temsirolimus has been tested in r/r PCNSL, but the overall response rate was only 54% (Korfel et al., 2016), and no further studies have been done. Myc protein was found to be expressed in 40-73% of PCNSL cases (Chang et al., 2003; Franco et al., 2014; Son et al., 2016; Yin et al., 2019), but also was not detected in any of the 27 cases evaluated in 1 study (Nozaki et al., 1998), indicating that the detection of Myc protein was not consistent across studies. Additionally, the prognostic significance of Myc protein expression was also inconsistent between studies, where 2 studies found that Myc protein expression was correlated with worse overall survival (Chang et al., 2003; Son et al., 2016) while 2 other studies found no such correlation (Franco et al., 2014; Yin et al., 2019). Myc mRNA expression was detected in 22% of PCNSL cases in 1 study (Son et al., 2016), and was highly expressed in PCNSL compared to non-CNS DLBCL (Rubenstein et al., 2006). Myc rearrangement was found in 7-8% of PCNSL cases (Brunn et al., 2013; Son et al., 2016). Based on these previous studies, it remains unclear whether Myc expression/rearrangement or mTOR activity can serve as prognostic markers of PCNSL.

We wondered whether the molecular response to ibrutinib was similar in other B cell malignancies. A previous study had identified the transcriptional response to ibrutinib in CLL patients, and found that ibrutinib strongly decreased the expression of B cell signature and oxidative phosphorylation genes, and less strongly the expression of NF-κB/TNFα and Myc-related genes, at 30 and 120 days post-ibrutinib therapy (Rendeiro et al., 2020). We also observed in our PDX

models that oxidative phosphorylation genes, in addition to NF-κB/TNFα and Myc-related genes, were down-regulated by ibrutinib, suggesting similarities in the molecular ibrutinib response in CLL and PCNSL but potential differences in the magnitude of the response. However, we can only speculate since there were considerable differences in the sample type (CLL: patient sample vs. PCNSL: PDX/cell line), method (CLL: single cell RNA-seq vs. PCNSL: bulk RNA-seq), and time point (CLL: months vs. PCNSL: hours). Thus, it will be curious as a future direction to evaluate the ibrutinib transcriptional response in previously established CLL, MCL, and WM models under our experimental conditions in order to compare the ibrutinib responses between PCNSL, CLL, MCL, and WM.

Mechanisms of resistance to ibrutinib in PCNSL

Since many PCNSL patients progressed on ibrutinib therapy, we investigated the mechanisms of ibrutinib resistance. We detected PLCG2 and CARD11 mutations in our PCNSL cell lines with acquired resistance and PCNSL patients in our study, but did not detect any mutations in BTK. This was intriguing since BTK mutations were detected very frequently in CLL patients, and also in MCL and WM patients at lower frequencies. PLCG2 mutations were observed in CLL, WM, and PCNSL (our study), but not in MCL patients. Moreover, CARD11 mutations were found in MCL, WM, and PCNSL (our study), but not in CLL patients.

It is curious that BCR pathway mutations in BTK, PLCG2, and CARD11 occurred at different frequencies, or not at all, in PCNSL, CLL, MCL, and WM

patients. It is possible that the different biology contributing to BTK dependency in each disease may influence the acquisition or frequency of these mutations leading to ibrutinib resistance. For example, CLL patients had constitutive BCR signaling with no defining genetic mutations, while PCNSL patients had frequent mutations in CD79B and MYD88 or other mechanism of BTK activation. CLL patients acquired BTK and/or PLCG2 mutations, while PCNSL patients had CARD11 and/or PLCG2 mutations, but no BTK mutations. Considering these findings, CLL appeared to have a greater dependence on the specific activity of BTK and/or PLCG2 in the pathway, and therefore CLL cells mutated these genes to restore pathway activity. On the other hand, PCNSL may have greater dependence on CARD11 and/or PLCG2 activity, and thus mutated these genes to become resistant to ibrutinib. It will be interesting to further study the specific dependencies on BCR pathway proteins in different B cell malignancies.

Additionally, it is unknown whether having more than 1 BCR pathway mutations (BTK/PLCG2 in CLL or CARD11/PLCG2 in PCNSL) confers greater resistance to ibrutinib. Our single cell cloning of the CNS11-RA cell line demonstrated that CARD11 and PLCG2 mutations were not mutually exclusive and suggested that having 1 (PLCG2) or both mutations did not affect the degree of biological resistance to ibrutinib. However, the CNS11-RA cell line also had additional mutations (PDS5B, ROBO1) that could confer resistance. Thus, further research will be needed to fully answer this question.

Several CARD11 mutations, such as K215M and D230N, were detected in both primary and acquired resistance settings in B cell malignancies, suggesting

that there was no difference between the mutations observed in these settings. However, there were also mutations that were seen only in primary resistance (T117P, R179Q), only in acquired resistance (R337Q, L878F), or in neither (M183L, S250P, D387V) (Bartlett et al., 2018; Lenz et al., 2008; L. Xu et al., 2017), indicating that there might be mutations associated with specifically primary or acquired resistance or were simply oncogenic.

Alternative mechanisms of primary and acquired ibrutinib resistance have been described in CLL, MCL, and WM. In CLL, histologic transformation has been observed in patients with primary resistance to ibrutinib (Ahn et al., 2017). Moreover, previous work found that nurse-like cells could protect CLL cells from the cytotoxic effects of ibrutinib by secreting IL10, resulting in primary drug resistance (Fiorcari et al., 2016; Guo et al., 2017). Deletion of chromosomes 8p, 11q, 13q, or 17p was associated with acquired ibrutinib resistance in CLL (J. A. Burger et al., 2016; Maddocks et al., 2015). Chromosome 8p contained the gene encoding tumor necrosis factor-related apoptosis-inducing ligand (TRAIL), a receptor required for TRAIL-mediated apoptosis. Thus, deletion of TRAIL resulted in impaired apoptosis associated with ibrutinib resistance (J. A. Burger et al., 2016). In MCL, primary resistance mechanisms included mutations in the BCR/NF-κB pathway (CARD11, RELA NF-κB subunit, tumor necrosis factor receptor-associated factor 6 (TRAF2), Baculoviral IAP repeat containing 3 (BIRC3)) (Jain et al., 2018; Rahal et al., 2013; Saba et al., 2016), mutations in cyclin D1 (Mohanty et al., 2016), or increased oxidative phosphorylation (L. Zhang et al., 2019). Acquired resistance occurred through integrin-β1 or stromal

cell-mediated activation of the PI3K/AKT pathway within the tumor microenvironment, promoting cell adhesion and resistance to ibrutinib in MCL (Guan, Huang, Yakimchuk, & Okret, 2018; Zhao et al., 2017). Another mechanism of acquired resistance in MCL is through mutation in tumor protein P53 (TP53) or ataxia telangiectasia mutated (ATM) (Jain et al., 2018). In WM, CXCR4 mutation has been associated with primary ibrutinib resistance by mediating activation of AKT and ERK signaling (Cao et al., 2014). Acquired resistance has been correlated with increased AKT or BCL-2 levels, and resistance can be overcome using AKT or BCL-2 inhibitors (Paulus et al., 2017).

It will be interesting to explore additional mechanisms of resistance in PCNSL. In the CNS11-RA PCNSL cell line with acquired resistance, we identified mutations in ROBO1 L487P and PDS5B L131F. Both of these genes encode tumor suppressor proteins that have not yet been implicated in studies of ibrutinib resistance, and it would be curious to characterize these mutations and their impact on resistance to ibrutinib in PCNSL.

Ibrutinib-based combinations to overcome CARD11 mutation-mediated resistance

In our characterization of specific CARD11 mutations (F130V, R179Q, R337Q) in PCNSL cell lines, we found that all CARD11 mutations restored MALT1 protease and mTOR activity, but NF-κB activity was not consistently restored. This was curious since previous studies showed that CARD11 mutations, including F130V, activated the NF-κB pathway (Chan et al., 2012;

64

Dong et al., 2011; Lenz et al., 2008; Watt et al., 2015). It is possible that the intrinsic dependencies on specific BCR pathway proteins in PCNSL cells contributed to stronger restoration of MALT1 and mTOR activity in ibrutinib-resistant PCNSL cells. Since MALT1 is known to signal through the CBM complex, CARD11 mutation-mediated resistance through MALT1 was not surprising. mTOR was shown to be downstream of CARD11 in T cells and DLBCL cells (Hamilton et al., 2014; Phelan et al., 2018), and we demonstrated that mTOR was regulated by BTK in PCNSL models. Thus, mTOR activation in CARD11-mutant cells was also reasonable, although it is still unclear the precise mechanism by which CARD11 mutation activated mTOR. Further studies will be needed to dissect the specific events mediating mTOR activation. Of note, we found that expression of CARD11 WT conferred slight resistance to ibrutinib, which was also reported in a previous study in DLBCL (Caeser et al., 2021).

MALT1 inhibition with the SCM-02-138 compound did not sensitize CARD11-mutant PCNSL cells to ibrutinib, even though this compound was previously shown to induce cell death in a DLBCL cell line mutant for CARD11 (Fontán et al., 2018). We confirmed that our PCNSL cells had basal MALT1 protease activity and that inhibition of MALT1 decreased the cleavage of its substrates, including BCL10 and Roquin. However, since MALT1 inhibition did not induce PCNSL cell death, we concluded that MALT1 inhibitor might not be effective to overcome CARD11 mutation-mediated resistance.

Ibrutinib combined with the mTOR inhibitor rapamycin, however, effectively induced cell death in CARD11-mutant cells, suggesting that mTOR

activity was important for the survival of these cells. Our biochemical analysis of the pathway showed that ibrutinib and rapamycin effectively inhibited BTK and mTORC1 activity. Although the mTOR inhibitor temsirolimus as a single agent elicited only a 54% overall response rate in r/r PCNSL (Korfel et al., 2016), reintroducing mTOR inhibitor in combination with ibrutinib specifically for CARD11-mutant PCNSL could be effective based on our findings. The combination of ibrutinib and mTOR inhibitor has previously been evaluated in ABC DLBCL (Ezell et al., 2014; Phelan et al., 2018) but is novel in the context of CARD11 mutation in PCNSL.

In thinking about proposing an mTOR inhibitor as therapy, an important consideration is the potential feedback re-activation of the pathway. For example, feedback re-activation of AKT has been observed with mTOR inhibitors, particularly rapalogs (O'Reilly et al., 2006). Our preliminary evidence demonstrated that rapamycin did not induce AKT phosphorylation at T308 at 12 h post-treatment in PCNSL cell lines. We also observed that ibrutinib alone or in combination with rapamycin effectively inhibited pAKT T308, suggesting that feedback activation, if any, may not be a concern in these cells. However to confirm these findings, further studies extending the treatment duration should be performed.

In addition to the ibrutinib and mTOR inhibitor combination, there are also other potential ibrutinib-based combinations that could be effective at targeting the pathway downstream of CARD11. For example, the bromodomain and extra-terminal motif (BET) inhibitor JQ1, which inhibits IKK activity, was shown to

synergize with ibrutinib in ABC DLBCL cell lines, including a CARD11-mutant cell line (Ceribelli et al., 2014). However, there have also been reported feedback activation mechanisms with IKK inhibition, where inhibition of IKKβ led to compensatory activation of IKKα (Lam et al., 2008). Thus, a thorough understanding of the pathway and how cells react to pathway inhibitors will be crucial to propose effective ibrutinib-based combinations to overcome resistance mediated by CARD11 mutations.

Conclusion

In summary, we have defined a molecular response to ibrutinib in novel PCNSL models, demonstrating that BTK inhibition decreased expression of genes involved in NF-κB/TNFα signaling and protein translation, suggesting that these processes were regulated downstream of BTK in PCNSL. Moreover, we have identified CARD11 and PLCG2 mutations as candidate ibrutinib resistance mutations in PCNSL cell lines and patients in our study. We further described a specific mechanism of resistance through mTOR in CARD11-mutant cells, which can be overcome with combined ibrutinib and mTOR inhibitor treatment.

CHAPTER 5: MATERIALS AND METHODS

PDX model derivation: Brain biopsy samples from untreated PCNSL patients were processed into a single cell suspension. Briefly, patient biopsy tissue was dissociated in Accumax Cell Dissociation Solution (Stemcell Technologies) and cells were filtered through a 100 µm filter. Cells were assessed for viability using the Vi-CELL XR cell viability analyzer (Beckman Coulter). The concentration of cells was adjusted to the desired amount (ex. 1×10^4 cells/µL/mouse) and engrafted into the right striatum of the brain of ICR-Prkdc^{SCID} mice (Taconic) by stereotaxic intracranial injection with Hamilton glass syringe. Mice were closely monitored for neurological symptoms and weight loss. ICR-Prkdc^{SCID} mice lack B and T cells due to a mutant DNA-dependent protein kinase, which cannot repair double stranded DNA breaks during V(D)J recombination.

PDX tumor cell injections in other mouse organs: ICR-Prkdc^{SCID} mice were injected with 1×10^6 cells/mouse into the right flank for subcutaneous injections, 1×10^6 cells/mouse into the peritoneum for intraperitoneal injections, or 2×10^6 cells/mouse into the tail vein for intravenous injections.

Immunohistochemistry (IHC): Tumor-bearing mouse brain was fixed in 10% formalin solution followed by 70% ethanol, and processed by the MSKCC Molecular Cytology Core to generate formalin-fixed paraffin-embedded (FFPE) tissue blocks. FFPE blocks were sectioned at 5 µm thickness on a microtome,

mounted onto microscope slides, and stained for various proteins using lab-optimized protocols on the Ventana automated slide stainer (Roche). The antibodies used for IHC were: CD20 (Dako/Agilent), Ki67 (Dako/Agilent), CD10 (Vector Laboratories), BCL-6 (GI191E/A8, Ventana/Roche), and MUM-1 (Dako/Agilent). H&E stains were performed with the MSKCC Molecular Cytology Core.

***In vivo* studies with ibrutinib:** Ibrutinib was synthesized by the MSKCC Organic Synthesis Core Facility (Core Head: Ouathek Ouerfelli), and dissolved in solvent containing 0.5% methylcellulose and 0.2% Tween-80. Ibrutinib was administered by oral gavage at a dose of 50 mg/kg per mouse for all experiments. Mice were randomized based on the order of injection to account for the freshness of cells at the time of injection. For studies with mice bearing intracranial tumors, survival was tracked in mice treated with ibrutinib starting 5 days post-injection and continued daily until the established endpoint (signs of neurological illness or loss of 20% body weight). For studies with mice bearing subcutaneous tumors, tumor volume was measured in mice treated with ibrutinib starting at the time when tumors were palpable and continued until tumors reached the maximum volume. For acute ibrutinib treatment studies, mice bearing both intracranial and subcutaneous tumors were treated at 22 days post-injection with ibrutinib for 2 h, and plasma, intracranial tumors, and subcutaneous tumors were collected for ibrutinib concentration measurements by LC-MS/MS (methods described below). To collect plasma, blood was first collected by cardiac puncture, dispensed into

tubes containing ethylenediaminetetraacetic acid (EDTA), and centrifuged at 1,400 rpm for 10 min at 4°C. Plasma was collected into clean eppendorf tubes and frozen at -80°C until analysis. Small samples of intracranial and subcutaneous tumor were processed for FFPE, and the rest of the tissue was snap frozen in liquid nitrogen and stored at -80°C until analysis.

Quantification of ibrutinib in mouse plasma and brain tissue by LC-MS/MS:
Ibrutinib standard (Cayman Chemical Company) was prepared at 1 mg/mL in ethanol and then further diluted in 50:50 methanol:water to prepare calibration curves from 2.5 ng/mL to 200 ng/mL for plasma samples and 0.2 – 25 ng/mL for tissue samples. Mouse plasma (50 µL) was extracted in 200 µL of ice-cold methanol and acetonitrile mixture (v/v = 1/1), incubated at -20°C for 1 h. Extracts were then centrifuged at 21,000 g for 10 minutes at 4°C and 100 µL of supernatant of transferred to a 96-well microplates (DWK-Wheaton, PN# 07-3000-300). Mouse brain tissue and subcutaneous tumor tissue were ground in liquid nitrogen to a fine powder and ~50-80 mg transferred into a cold 2-mL BeadRuptor tube containing 2.8 mm ceramic beads (Omni International, PN# 19-628). Extraction solvent (v/v 4/4/2 = acetonitrile/methanol/water) was added for a final concentration of 50 mg/mL and samples were homogenized for 3 min at 16 m/s at 4°C. Extracts were then centrifuged at 21,000 g for 10 minutes at 4°C and 100 µL of supernatant of transferred to a 96-well microplates. Quality control (QC) samples were prepared from rat brain tissue and mouse plasma and 10 uL d5-Ibrutinib internal standard (Cayman Chemical Company, Ann Arbor, MI, USA)

was added to all calibrators, QC and samples and mixed by pipetting. LC-MS-MS analysis was performed on a SCIEX API-4000 triple quadrupole mass spectrometer (SCIEX) equipped with a Shimadzu Prominence HPLC (Shimadzu Corp.). Chromatographic separation used a XBridge C18, 3.5 µm, 50×2.1 mm column (Waters, Part # 186003021). Mobile phase A was water with 0.1% formic acid, mobile phase B was 100% acetonitrile. Injection volume was 5 µL and the HPLC gradient was: 0 min, 35% B; 1 min, 35% B; 4 min, 95% B; 4.5 min 95% B; 5 min 35% B with 2.5 min re-equilibration. Analyte and ISTD eluted at 2.6 min. API4000 MS parameters were: CUR, 35 psi; Gas 1, 35 psi; Gas 2, 65 psi; IS, 4500 V; TEM, 500°C; CAD, 12 psi, operating in positive ionization mode. Ibrutinib was monitored at m/z 441.2 → 138.1* and 441.2 → 304.1, Ibrutinib-d5 using m/z 446.2 → 138.1* and 446.2 → 309.1, with * indicating the primary transition used for quantitation. Data was processed using Analyst 1.6.2 software (SCIEX) with a 1/x weighting on all calibration curves. QC samples were confirmed to have accuracy and CV within 15%.

***Ex vivo* tissue slice culture assay**: PDX mouse brains were dissected and mounted onto a vibratome (Leica) and suspended in ice-cold phosphate buffered saline (PBS) (MSKCC Media Core Facility). Brains were sectioned at 300 µm thickness and plated on Millicell culture plate inserts (EMD Millipore) in 6-well plates. The tissue slices were treated with 1 mL of drug diluted in media (RPMI (MSKCC Media Core Facility) supplemented with 5% fetal bovine serum (FBS) (Omega Scientific, Inc) and 1% penicillin:streptomycin solution (Gemini Bio-

Products)) and incubated in a cell culture incubator at 37°C with 5% CO_2. Tissue slices were collected on dry ice into clean eppendorf tubes and frozen at -80°C until analysis.

Cell culture: The PCNS#11 cell line was cultured in RPMI (MSKCC Media Core Facility) supplemented with 5% FBS (Omega Scientific, Inc) and 1% penicillin:streptomycin solution (Gemini Bio-Products). Human embryonic kidney (HEK) 293T cells were cultured in DMEM-High glucose (MSKCC Media Core Facility) supplemented with 10% FBS (Omega Scientific, Inc) and 1% penicillin:streptomycin solution (Gemini Bio-Products). All cell lines were grown in a 37°C cell culture incubator with 5% CO_2. Cell media was replaced every 3 to 4 days.

Single cell cloning: To generate conditioned media for single cell cloning, cells were first seeded at 50-60% confluence and incubated overnight. The next day, cells were centrifuged at 1,300 rpm for 2 min and the supernatant (conditioned media) was collected into a clean 15 mL conical tube. Cells were resuspended in fresh media and counted using the Vi-CELL XR cell viability analyzer (Beckman Coulter). The cell concentration was diluted to 5 cells/mL (50 cells/10 mL) with conditioned media, and 100 µL of this cell solution was plated into each well of a 96-well plate so that there were 0-1 cells per well. Each well was checked by microscopy for presence of a single cell, and the wells with single cells were marked. Cells were incubated in a 37°C cell culture incubator with 5% CO_2 for 7-

14 days, and wells were checked for cell growth. Single cells that grew out were expanded and collected for DNA extraction and sequencing.

DNA sequencing and genomic analysis: DNA was extracted from cells or tissue using the DNeasy Blood and Tissue Kit (QIAGEN) and quantified using the Nanodrop spectrophotometer (Thermo Fisher Scientific). Targeted gene sequencing was performed with the MSKCC Integrated Genomics Operation (IGO) HemePACT panel of 576 genes implicated in hematological malignancies. Data were processed by the MSKCC Bioinformatics Core (BIC) and deposited into cBioportal (Cerami et al., 2012; Gao et al., 2013). Array comparative genomic hybridization (aCGH) was performed using a protocol from Agilent Technologies, and data were analyzed with Agilent Cytogenomics software version 1.5, as previously described (Grommes et al., 2017).

RNA sequencing and analysis: RNA was extracted from cells or tissue using the RNeasy Mini Kit (QIAGEN) and quantified using the Nanodrop spectrophotometer (Thermo Fisher Scientific). RNA sequencing (paired-end 50 (PE50), poly-A) was performed at the MSKCC IGO core facility. Sequencing reads were processed and aligned by the MSKCC BIC. Differential gene expression analysis was performed using the Bioconductor package DESeq2 in RStudio. Gene ontology analysis was performed using the GSEA software version 4.1.0 (Broad Institute) for enrichment of the Molecular Signatures

Database (MSigDB) Hallmark and C2 curated gene sets (Liberzon et al., 2015; Mootha et al., 2003; Subramanian et al., 2005).

DNA cloning: The retroviral empty vector backbone pMSCV Puro IRES GFP (MPIG) (Plasmid # 21654), and Gateway donor vectors pDONR223 BTK (Plasmid #23918) and pDONR223 CARD11 (Plasmid #23482) were purchased from Addgene. PCR primers were designed using the In-Fusion Cloning Primer Design Tool, and then manually designed to append an HA tag to the C-terminus of each protein. BTK or CARD11 gene inserts were amplified from pDONR223 BTK or pDONR223 CARD11, respectively, by polymerase chain reaction (PCR) using the CloneAmp HiFi PCR Premix (Takara Bio). PCR products (gene inserts) were run on a 1% agarose gel to confirm band size. Bands of correct sizes were excised and gel purified using the NucleoSpin PCR Clean-up kit (Takara Bio). MPIG empty vector was linearized by restriction enzyme digestion (XhoI for BTK or EcoRI for CARD11) depending on the gene insertion site. Purified gene inserts were cloned into the linearized vector by In-Fusion HD Cloning Plus enzyme (Takara Bio) and transformed into One Shot TOP10 competent cells (Thermo Fisher Scientific) using a standard transformation protocol. DNA from bacterial colonies was extracted using the QIAprep Spin Miniprep Kit (QIAGEN) and sequenced (GeneWiz Sanger sequencing) to confirm proper cloning of the gene into the vector. DNA was then amplified in bacteria and isolated using the HiSpeed Plasmid Maxi kit (QIAGEN). DNA concentrations were determined using the Nanodrop Spectrophotometer (Thermo Fisher Scientific).

Site-directed mutagenesis: Mutagenesis primers were designed using the QuikChange Primer Design tool (Agilent Technologies). The QuikChange Lightning kit (Agilent) was used to generate point mutations in BTK or CARD11 following the standard protocol for mutagenesis and transformation into XL10-Gold ultracompetent cells. To confirm that the correct mutation was generated, DNA from bacterial colonies was extracted using the QIAprep Spin Miniprep Kit (QIAGEN) and sequenced (GeneWiz Sanger sequencing). DNA was then amplified in bacteria and isolated using the HiSpeed Plasmid Maxi kit (QIAGEN). DNA concentrations were determined using the Nanodrop Spectrophotometer (Thermo Fisher Scientific).

Virus generation and cell transduction: Retrovirus particles were produced in HEK 293T cells and used to introduce DNA into target PCNSL cells. This protocol was adapted from the Titia de Lange Lab at The Rockefeller University. Briefly, HEK 293T cells were seeded at 10-20% confluence on Day 1 (am). On Day 2 (pm), HEK 293T cells were transfected with X-tremeGENE HP DNA Transfection Reagent (Sigma-Aldrich) with 2.5 ug of plasmid DNA and 2.5 ug of the retroviral packaging plasmid pCL-Ampho. Media was discarded and replaced on Day 3 (am and pm). On Day 4, virus supernatant was collected and media was replaced on HEK 293T cells to continue virus production. Virus supernatant was then filtered through a 0.22 μm filter, and immediately used to transduce target PCNSL cells. PCNSL cells (1.5×10^5 cells per well in a 6-well plate) were

resuspended in 1 mL of fresh virus with 4 μg/mL of polybrene (Santa Cruz Biotechnology) and incubated overnight. The following day (Day 5), virus supernatent was again collected from HEK 293T cells, and PCNSL cells were infected with fresh virus two more times (am and pm). On Day 8, PCNSL cells were removed from virus and resuspended in fresh media with 0.1 μg/mL of puromycin (Invivogen). PCNSL cells were selected for 1 month and maintained in 0.1 μg/mL of puromycin.

Drugs for *ex vivo* and *in vitro* studies: For *ex vivo* and *in vitro* studies, ibrutinib was synthesized by the MSKCC Organic Synthesis Core Facility (Core Head: Ouathek Ouerfelli). For *in vitro* studies, ibrutinib (catalog #: S2680) and rapamycin (catalog #: S1039) were purchased from Selleckchem. The MALT1 inhibitor, SCM-02-138, was from Ari Melnick at Weill Cornell Medical College. All drugs were reconstituted and diluted in DMSO.

Flow cytometry: Cells (1.5×10^5 per condition) were treated with drug in 6 cm plates for 4 days and collected by centrifugation at 1,300 rpm for 2 min at room temperature (RT). Cells were washed with PBS (MSKCC Media Core Facility) and collected by centrifugation at 1,300 rpm for 2 min at RT. Cells were resuspended in 100 μL of Annexin-binding buffer containing 50 mM HEPES, 700 mM NaCl, and 12.5 mM $CaCl_2$ at pH 7.4 (Thermo Fisher Scientific). Propidium iodide (PI) was added (1 μL of 100 μg/mL stock) (Thermo Fisher Scientific) and cells were incubated for 15 min at RT. Cells were then diluted into 400 μL of

Annexin-binding buffer and analyzed by flow cytometry (Fortessa 2, MSKCC

Flow Cytometry Core Facility). Results were analyzed using FlowJo 3 and

graphed using GraphPad Prism version 7.0a.

Vi-CELL viability assay: Cells (1.5×10^5 per condition) were treated with drug in

6 cm plates for 4 days and collected by centrifugation at 1,300 rpm for 2 min at

RT. Cells were washed with PBS (MSKCC Media Core Facility) and collected by

centrifugation at 1,300 rpm for 2 min at RT. Cells were resuspended in 1 mL of

media and analyzed on the Vi-CELL ("Vi-Sheen") XR cell viability analyzer

(Beckman Coulter). Cell viability was determined by Trypan blue dye exclusion.

Results were analyzed in Microsoft Excel and graphed using GraphPad Prism

version 7.0a.

Western blot: For *ex vivo* experiments, tissue was treated with drug, collected

directly into 1.5 mL eppendorf tubes on dry ice, and stored at -80°C until lysis.

For *in vitro* experiments, cells (1×10^6 per condition) were treated with drug and

collected by centrifugation at 1,300 rpm for 2 min at RT. Cells were washed with

PBS (MSKCC Media Core Facility) and collected by centrifugation at 1,300 rpm

for 2 min at RT. Tissue (*ex vivo* experiments) or cells (*in vitro* experiments) were

resuspended in 300 µL of lysis buffer (1X Cell Lysis Buffer (Cell Signaling

Technology), 1% protease inhibitor cocktail set III (Calbiochem), 1%

phosphatase inhibitor cocktail set II (Calbiochem)). Cells were then sonicated

using the Sonic Dismembrator Model 500 (Thermo Fisher Scientific) and

centrifuged at 13,000 rpm for 10 min at 4°C. Supernatents containing the cell lysates were collected into clean 1.5 mL eppendorf tubes and kept on ice. Protein was quantified using the DC Protein Assay (Bio-Rad) and protein concentrations were standardized across all samples. Lysates were prepared with Laemmli SDS reducing sample buffer (Boston BioProducts), boiled for 5 min at 100°C, and centrifuged briefly to collect condensation. Samples were loaded on 4 - 15% Criterion Tris-HCl gradient gels (Bio-Rad) and run at constant amperage of 0.05 A in running buffer (Tris, Glycine, 10% sodium dodecyl sulfate (SDS)). Proteins were transferred to 0.45 μm nitrocellulose blotting membranes (GE Healthcare) at constant voltage of 80 V for 2 h at 4°C in transfer buffer (Tris 25 mM, Glycine 192 mM, 20% methanol). Nitrocellulose membranes were stained with Ponceau S (0.1% w/v in 5% acetic acid) and rinsed with dH_2O. Membranes were blocked for 30 min with 5% nonfat dry milk (Lab Scientific) dissolved in TBS-T (TBS (Tris, sodium chloride) with 0.1% Tween 20 (Thermo Fisher Scientific)). Primary antibodies diluted in 5% nonfat dry milk were added to the membranes and incubated at 4°C overnight on a shaker. The next day, membranes were washed with TBS-T for 30 min (replacing TBS-T every 10 min) on a shaker at RT, incubated with secondary antibody diluted in 5% nonfat dry milk for 1 h on a shaker at RT, and washed again with TBS-T for 30 min (replacing TBS-T every 10 min) on a shaker at RT. Membranes were developed using ECL Western Blotting Detection Reagent (GE Healthcare) and ECL Prime Western Blotting Detection Reagent (GE Healthcare) as instructed. Chemiluminescence was detected using a film processor (Konica Minolta). X-ray films were scanned using

the Epson Perfection V600 photo scanner and analyzed in Adobe Photoshop. Densitometry of bands was assessed using ImageJ software, and figures were made in Microsoft PowerPoint.

Western blot antibodies: The following antibodies were used: CD20 (Dako/Agilent), β-Actin (8H10D10-CST), Vinculin XP (E1E9V-CST), cleaved PARP Asp214 (19F4-CST), cleaved caspase-3 Asp175 (9661S-CST), anti-HA ((3F10-Roche), p-BTK Y223 (EP420Y-Abcam), BTK (D3H5-CST), p-CARD11 S652 (5189S-CST), CARD11 (1D12-CST), p-IKKα/β S176/180 (16A6-CST), IKKα (3G12-CST), IKKβ (D30C6-CST), p-IκBα S32/36 (9246S-CST), IκBα (L35A5-CST), p-NFκB p65 S536 (93H1-CST), NFκB p65 XP (D14E12-CST), pAKT S473 XP (D9E-CST), pAKT T308 XP (D25E6-CST), AKT (4691L-CST), p-PRAS40 T246 (C77D7-CST), PRAS40 (2610S-CST), p-p70 S6K T389 (9205S-CST), p70 S6K (9202S-CST), pS6 S235/236 (2211S-CST), pS6 S240/244 (2215S-CST), S6 RP (5G10-CST), p4EBP1 T37/46 (236B4-CST), 4EBP1 (53H11-CST), c-Myc (D84C12-CST), Anti-Roquin-1/2 (3F12-Millipore Sigma), Anti-Bcl10 (EP606Y-Abcam). CST: Cell Signaling Technology.

REFERENCES

Ahn, I. E., Underbayev, C., Albitar, A., Herman, S. E., Tian, X., Maric, I., . . . Wiestner, A. (2017). Clonal evolution leading to ibrutinib resistance in chronic lymphocytic leukemia. *Blood, 129*(11), 1469-1479. doi:10.1182/blood-2016-06-719294

Alessi, D. R., James, S. R., Downes, C. P., Holmes, A. B., Gaffney, P. R., Reese, C. B., & Cohen, P. (1997). Characterization of a 3-phosphoinositide-dependent protein kinase which phosphorylates and activates protein kinase Balpha. *Curr Biol, 7*(4), 261-269. doi:10.1016/s0960-9822(06)00122-9

Alizadeh, A. A., Eisen, M. B., Davis, R. E., Ma, C., Lossos, I. S., Rosenwald, A., . . . Staudt, L. M. (2000). Distinct types of diffuse large B-cell lymphoma identified by gene expression profiling. *Nature, 403*(6769), 503-511. doi:10.1038/35000501

Baba, Y., Hashimoto, S., Matsushita, M., Watanabe, D., Kishimoto, T., Kurosaki, T., & Tsukada, S. (2001). BLNK mediates Syk-dependent Btk activation. *Proc Natl Acad Sci U S A, 98*(5), 2582-2586. doi:10.1073/pnas.051626198

Bartlett, N. L., Costello, B. A., LaPlant, B. R., Ansell, S. M., Kuruvilla, J. G., Reeder, C. B., . . . Fehniger, T. A. (2018). Single-agent ibrutinib in relapsed or refractory follicular lymphoma: a phase 2 consortium trial. *Blood, 131*(2), 182-190. doi:10.1182/blood-2017-09-804641

Beg, A. A., Ruben, S. M., Scheinman, R. I., Haskill, S., Rosen, C. A., & Baldwin, A. S., Jr. (1992). I kappa B interacts with the nuclear localization sequences of the subunits of NF-kappa B: a mechanism for cytoplasmic retention. *Genes Dev, 6*(10), 1899-1913. doi:10.1101/gad.6.10.1899

Berridge, M. J. (1993). Inositol trisphosphate and calcium signalling. *Nature, 361*(6410), 315-325. doi:10.1038/361315a0

Brunn, A., Nagel, I., Montesinos-Rongen, M., Klapper, W., Vater, I., Paulus, W., . . . Deckert, M. (2013). Frequent triple-hit expression of MYC, BCL2, and BCL6 in primary lymphoma of the central nervous system and absence of a favorable MYClowBCL2low subgroup may underlie the inferior prognosis as compared to systemic diffuse large B cell lymphomas. *Acta Neuropathologica, 126*(4), 603-605. doi:10.1007/s00401-013-1169-7

Burger, J. A., Landau, D. A., Taylor-Weiner, A., Bozic, I., Zhang, H., Sarosiek, K., . . . Wu, C. J. (2016). Clonal evolution in patients with chronic lymphocytic leukaemia developing resistance to BTK inhibition. *Nat Commun, 7*, 11589. doi:10.1038/ncomms11589

Burger, J. A., Tedeschi, A., Barr, P. M., Robak, T., Owen, C., Ghia, P., . . . Kipps, T. J. (2015). Ibrutinib as Initial Therapy for Patients with Chronic Lymphocytic Leukemia. *New England Journal of Medicine, 373*(25), 2425-2437. doi:10.1056/NEJMoa1509388

Byrd, J. C., Furman, R. R., Coutre, S. E., Flinn, I. W., Burger, J. A., Blum, K. A., . . . O'Brien, S. (2013). Targeting BTK with Ibrutinib in Relapsed Chronic

Lymphocytic Leukemia. *New England Journal of Medicine, 369*(1), 32-42. doi:10.1056/NEJMoa1215637

Byrd, J. C., Harrington, B., O'Brien, S., Jones, J. A., Schuh, A., Devereux, S., . . . Furman, R. R. (2016). Acalabrutinib (ACP-196) in Relapsed Chronic Lymphocytic Leukemia. *New England Journal of Medicine, 374*(4), 323-332. doi:10.1056/NEJMoa1509981

Caeser, R., Walker, I., Gao, J., Shah, N., Rasso-Barnett, L., Anand, S., . . . Hodson, D. J. (2021). Acquired CARD11 mutation promotes BCR independence in Diffuse Large B Cell Lymphoma. *JCO Precis Oncol, 5*, 145-152. doi:10.1200/PO.20.00360

Cao, Y., Hunter, Z. R., Liu, X., Xu, L., Yang, G., Chen, J., . . . Treon, S. P. (2014). The WHIM-like CXCR4S338X somatic mutation activates AKT and ERK, and promotes resistance to ibrutinib and other agents used in the treatment of Waldenstrom's Macroglobulinemia. *Leukemia, 29*(1), 169-176. doi:10.1038/leu.2014.187

Cerami, E., Gao, J., Dogrusoz, U., Gross, B. E., Sumer, S. O., Aksoy, B. A., . . . Schultz, N. (2012). The cBio Cancer Genomics Portal: An Open Platform for Exploring Multidimensional Cancer Genomics Data: Figure 1. *Cancer Discovery, 2*(5), 401-404. doi:10.1158/2159-8290.cd-12-0095

Ceribelli, M., Kelly, P. N., Shaffer, A. L., Wright, G. W., Xiao, W., Yang, Y., . . . Staudt, L. M. (2014). Blockade of oncogenic I B kinase activity in diffuse large B-cell lymphoma by bromodomain and extraterminal domain protein inhibitors. *Proceedings of the National Academy of Sciences, 111*(31), 11365-11370. doi:10.1073/pnas.1411701111

Chan, W., Schaffer, T. B., & Pomerantz, J. L. (2012). A Quantitative Signaling Screen Identifies CARD11 Mutations in the CARD and LATCH Domains That Induce Bcl10 Ubiquitination and Human Lymphoma Cell Survival. *Molecular and Cellular Biology, 33*(2), 429-443. doi:10.1128/mcb.00850-12

Chang, C. C., Kampalath, B., Schultz, C., Bunyi-Teopengco, E., Logan, B., Eshoa, C., . . . Perkins, S. L. (2003). Expression of p53, c-Myc, or Bcl-6 suggests a poor prognosis in primary central nervous system diffuse large B-cell lymphoma among immunocompetent individuals. *Arch Pathol Lab Med, 127*(2), 208-212. doi:10.5858/2003-127-208-EOPMOB

Chapuy, B., Roemer, M. G., Stewart, C., Tan, Y., Abo, R. P., Zhang, L., . . . Shipp, M. A. (2016). Targetable genetic features of primary testicular and primary central nervous system lymphomas. *Blood, 127*(7), 869-881. doi:10.1182/blood-2015-10-673236

Chapuy, B., Stewart, C., Dunford, A. J., Kim, J., Kamburov, A., Redd, R. A., . . . Shipp, M. A. (2018). Molecular subtypes of diffuse large B cell lymphoma are associated with distinct pathogenic mechanisms and outcomes. *Nature Medicine, 24*(5), 679-690. doi:10.1038/s41591-018-0016-8

Chauvin, C., Koka, V., Nouschi, A., Mieulet, V., Hoareau-Aveilla, C., Dreazen, A., . . . Pende, M. (2014). Ribosomal protein S6 kinase activity controls the ribosome biogenesis transcriptional program. *Oncogene, 33*(4), 474-483. doi:10.1038/onc.2012.606

Chung, J. K., Nocka, L. M., Decker, A., Wang, Q., Kadlecek, T. A., Weiss, A., . . . Groves, J. T. (2019). Switch-like activation of Bruton's tyrosine kinase by membrane-mediated dimerization. *Proc Natl Acad Sci U S A, 116*(22), 10798-10803. doi:10.1073/pnas.1819309116

Correction for Pourdehnad et al., Myc and mTOR converge on a common node in protein synthesis control that confers synthetic lethality in Myc-driven cancers. (2013). *Proceedings of the National Academy of Sciences, 110*(42), 17160-17160. doi:10.1073/pnas.1317701110

Csibi, A., Lee, G., Yoon, S. O., Tong, H., Ilter, D., Elia, I., . . . Blenis, J. (2014). The mTORC1/S6K1 pathway regulates glutamine metabolism through the eIF4B-dependent control of c-Myc translation. *Curr Biol, 24*(19), 2274-2280. doi:10.1016/j.cub.2014.08.007

de Weers, M., Brouns, G. S., Hinshelwood, S., Kinnon, C., Schuurman, R. K., Hendriks, R. W., & Borst, J. (1994). B-cell antigen receptor stimulation activates the human Bruton's tyrosine kinase, which is deficient in X-linked agammaglobulinemia. *J Biol Chem, 269*(39), 23857-23860. Retrieved from https://www.ncbi.nlm.nih.gov/pubmed/7929028

Denes, V., Pilichowska, M., Makarovskiy, A., Carpinito, G., & Geck, P. (2010). Loss of a cohesin-linked suppressor APRIN (Pds5b) disrupts stem cell programs in embryonal carcinoma: an emerging cohesin role in tumor suppression. *Oncogene, 29*(23), 3446-3452. doi:10.1038/onc.2010.100

Dong, G., Chanudet, E., Zeng, N., Appert, A., Chen, Y.-W., Au, W.-Y., . . . Du, M.-Q. (2011). A20, ABIN-1/2, and CARD11 Mutations and Their Prognostic Value in Gastrointestinal Diffuse Large B-Cell Lymphoma. *Clinical Cancer Research, 17*(6), 1440-1451. doi:10.1158/1078-0432.ccr-10-1859

Dutil, E. M., Toker, A., & Newton, A. C. (1998). Regulation of conventional protein kinase C isozymes by phosphoinositide-dependent kinase 1 (PDK-1). *Curr Biol, 8*(25), 1366-1375. doi:10.1016/s0960-9822(98)00017-7

Epperla, N., Shana'ah, A. Y., Jones, D., Christian, B. A., Ayyappan, S., Maddocks, K., & Woyach, J. A. (2019). Resistance mechanism for ibrutinib in marginal zone lymphoma. *Blood Adv, 3*(4), 500-502. doi:10.1182/bloodadvances.2018029058

Erdmann, T., Klener, P., Lynch, J. T., Grau, M., Vockova, P., Molinsky, J., . . . Lenz, G. (2017). Sensitivity to PI3K and AKT inhibitors is mediated by divergent molecular mechanisms in subtypes of DLBCL. *Blood, 130*(3), 310-322. doi:10.1182/blood-2016-12-758599

Ezell, S. A., Mayo, M., Bihani, T., Tepsuporn, S., Wang, S., Passino, M., . . . Byth, K. F. (2014). Synergistic induction of apoptosis by combination of BTK and dual mTORC1/2 inhibitors in diffuse large B cell lymphoma. *Oncotarget, 5*(13), 4990-5001. doi:10.18632/oncotarget.2071

Fiorcari, S., Maffei, R., Audrito, V., Martinelli, S., Ten Hacken, E., Zucchini, P., . . . Marasca, R. (2016). Ibrutinib modifies the function of monocyte/macrophage population in chronic lymphocytic leukemia. *Oncotarget, 7*(40), 65968-65981. doi:10.18632/oncotarget.11782

Fontán, L., Qiao, Q., Hatcher, J. M., Casalena, G., Us, I., Teater, M., . . . Melnick, A. (2018). Specific covalent inhibition of MALT1 paracaspase suppresses B cell lymphoma growth. *Journal of Clinical Investigation, 128*(10), 4397-4412. doi:10.1172/jci99436

Fox, L., Yannakou, C., Ryland, G., Lade, S., Dickinson, M., Campbell, B., & Prince, H. (2018). Molecular Mechanisms of Disease Progression in Primary Cutaneous Diffuse Large B-Cell Lymphoma, Leg Type during Ibrutinib Therapy. *International Journal of Molecular Sciences, 19*(6), 1758. doi:10.3390/ijms19061758

Franco, R., Gill, K. Z., Iwamoto, F., Allen, A., Hoehn, D., Murty, V. V., . . . Bhagat, G. (2014). MYC Protein Expression in Primary Diffuse Large B-Cell Lymphoma of the Central Nervous System. *PLoS ONE, 9*(12), e114398. doi:10.1371/journal.pone.0114398

Fruman, D. A., Chiu, H., Hopkins, B. D., Bagrodia, S., Cantley, L. C., & Abraham, R. T. (2017). The PI3K Pathway in Human Disease. *Cell, 170*(4), 605-635. doi:10.1016/j.cell.2017.07.029

Gao, J., Aksoy, B. A., Dogrusoz, U., Dresdner, G., Gross, B., Sumer, S. O., . . . Schultz, N. (2013). Integrative analysis of complex cancer genomics and clinical profiles using the cBioPortal. *Sci Signal, 6*(269), pl1. doi:10.1126/scisignal.2004088

Gold, M. R., Law, D. A., & DeFranco, A. L. (1990). Stimulation of protein tyrosine phosphorylation by the B-lymphocyte antigen receptor. *Nature, 345*(6278), 810-813. doi:10.1038/345810a0

Gold, M. R., Matsuuchi, L., Kelly, R. B., & DeFranco, A. L. (1991). Tyrosine phosphorylation of components of the B-cell antigen receptors following receptor crosslinking. *Proc Natl Acad Sci U S A, 88*(8), 3436-3440. doi:10.1073/pnas.88.8.3436

Grommes, C., & DeAngelis, L. M. (2017). Primary CNS Lymphoma. *J Clin Oncol, 35*(21), 2410-2418. doi:10.1200/JCO.2017.72.7602

Grommes, C., Pastore, A., Palaskas, N., Tang, S. S., Campos, C., Schartz, D., . . . Mellinghoff, I. K. (2017). Ibrutinib Unmasks Critical Role of Bruton Tyrosine Kinase in Primary CNS Lymphoma. *Cancer Discov, 7*(9), 1018-1029. doi:10.1158/2159-8290.CD-17-0613

Grommes, C., Tang, S. S., Wolfe, J., Kaley, T. J., Daras, M., Pentsova, E. I., . . . Mellinghoff, I. K. (2019). Phase 1b trial of an ibrutinib-based combination therapy in recurrent/refractory CNS lymphoma. *Blood, 133*(5), 436-445. doi:10.1182/blood-2018-09-875732

Guan, J., Huang, D., Yakimchuk, K., & Okret, S. (2018). p110α Inhibition Overcomes Stromal Cell–Mediated Ibrutinib Resistance in Mantle Cell Lymphoma. *Molecular Cancer Therapeutics, 17*(5), 1090-1100. doi:10.1158/1535-7163.mct-17-0784

Guo, A., Lu, P., Coffey, G., Conley, P., Pandey, A., & Wang, Y. L. (2017). Dual SYK/JAK inhibition overcomes ibrutinib resistance in chronic lymphocytic leukemia: Cerdulatinib, but not ibrutinib, induces apoptosis of tumor cells protected by the microenvironment. *Oncotarget, 8*(8), 12953-12967. doi:10.18632/oncotarget.14588

Hamilton, K. S., Phong, B., Corey, C., Cheng, J., Gorentla, B., Zhong, X., . . . Kane, L. P. (2014). T cell receptor-dependent activation of mTOR signaling in T cells is mediated by Carma1 and MALT1, but not Bcl10. *Sci Signal, 7*(329), ra55. doi:10.1126/scisignal.2005169

Hans, C. P. (2004). Confirmation of the molecular classification of diffuse large B-cell lymphoma by immunohistochemistry using a tissue microarray. *Blood, 103*(1), 275-282. doi:10.1182/blood-2003-05-1545

Holz, M. K., Ballif, B. A., Gygi, S. P., & Blenis, J. (2005). mTOR and S6K1 mediate assembly of the translation preinitiation complex through dynamic protein interchange and ordered phosphorylation events. *Cell, 123*(4), 569-580. doi:10.1016/j.cell.2005.10.024

Honigberg, L. A., Smith, A. M., Sirisawad, M., Verner, E., Loury, D., Chang, B., . . . Buggy, J. J. (2010). The Bruton tyrosine kinase inhibitor PCI-32765 blocks B-cell activation and is efficacious in models of autoimmune disease and B-cell malignancy. *Proc Natl Acad Sci U S A, 107*(29), 13075-13080. doi:10.1073/pnas.1004594107

Jain, P., Kanagal-Shamanna, R., Zhang, S., Ahmed, M., Ghorab, A., Zhang, L., . . . Wang, M. L. (2018). Long-term outcomes and mutation profiling of patients with mantle cell lymphoma (MCL) who discontinued ibrutinib. *British Journal of Haematology, 183*(4), 578-587. doi:10.1111/bjh.15567

Jefferies, C. A., Doyle, S., Brunner, C., Dunne, A., Brint, E., Wietek, C., . . . O'Neill, L. A. (2003). Bruton's tyrosine kinase is a Toll/interleukin-1 receptor domain-binding protein that participates in nuclear factor kappaB activation by Toll-like receptor 4. *J Biol Chem, 278*(28), 26258-26264. doi:10.1074/jbc.M301484200

Jiang, Z., Liang, G., Xiao, Y., Qin, T., Chen, X., Wu, E., . . . Wang, Z. (2019). Targeting the SLIT/ROBO pathway in tumor progression: molecular mechanisms and therapeutic perspectives. *Therapeutic Advances in Medical Oncology, 11*, 175883591985523. doi:10.1177/1758835919855238

Jones, D., Woyach, J. A., Zhao, W., Caruthers, S., Tu, H., Coleman, J., . . . Lozanski, G. (2017). PLCG2 C2 domain mutations co-occur with BTK and PLCG2 resistance mutations in chronic lymphocytic leukemia undergoing ibrutinib treatment. *Leukemia, 31*(7), 1645-1647. doi:10.1038/leu.2017.110

Khodabakhshi, A. H., Morin, R. D., Fejes, A. P., Mungall, A. J., Mungall, K. L., Bolger-Munro, M., . . . Jones, S. J. (2012). Recurrent targets of aberrant somatic hypermutation in lymphoma. *Oncotarget, 3*(11), 1308-1319. doi:10.18632/oncotarget.653

Kim, Y. J., Sekiya, F., Poulin, B., Bae, Y. S., & Rhee, S. G. (2004). Mechanism of B-cell receptor-induced phosphorylation and activation of phospholipase C-gamma2. *Mol Cell Biol, 24*(22), 9986-9999. doi:10.1128/MCB.24.22.9986-9999.2004

Korfel, A., Schlegel, U., Herrlinger, U., Dreyling, M., Schmidt, C., von Baumgarten, L., . . . Kiewe, P. (2016). Phase II Trial of Temsirolimus for Relapsed/Refractory Primary CNS Lymphoma. *Journal of Clinical Oncology, 34*(15), 1757-1763. doi:10.1200/jco.2015.64.9897

Krumbholz, M., Theil, D., Derfuss, T., Rosenwald, A., Schrader, F., Monoranu, C.-M., . . . Meinl, E. (2005). BAFF is produced by astrocytes and up-regulated in multiple sclerosis lesions and primary central nervous system lymphoma. *Journal of Experimental Medicine, 201*(2), 195-200. doi:10.1084/jem.20041674

Kurosaki, T., & Kurosaki, M. (1997). Transphosphorylation of Bruton's tyrosine kinase on tyrosine 551 is critical for B cell antigen receptor function. *J Biol Chem, 272*(25), 15595-15598. doi:10.1074/jbc.272.25.15595

Lam, L. T., Davis, R. E., Ngo, V. N., Lenz, G., Wright, G., Xu, W., . . . Staudt, L. M. (2008). Compensatory IKK activation of classical NF- B signaling during IKK inhibition identified by an RNA interference sensitization screen. *Proceedings of the National Academy of Sciences, 105*(52), 20798-20803. doi:10.1073/pnas.0806491106

Lamason, R. L., McCully, R. R., Lew, S. M., & Pomerantz, J. L. (2010). Oncogenic CARD11 Mutations Induce Hyperactive Signaling by Disrupting Autoinhibition by the PKC-Responsive Inhibitory Domain. *Biochemistry, 49*(38), 8240-8250. doi:10.1021/bi101052d

Lenz, G., Davis, R. E., Ngo, V. N., Lam, L., George, T. C., Wright, G. W., . . . Staudt, L. M. (2008). Oncogenic CARD11 mutations in human diffuse large B cell lymphoma. *Science, 319*(5870), 1676-1679. doi:10.1126/science.1153629

Liberzon, A., Birger, C., Thorvaldsdóttir, H., Ghandi, M., Mesirov, Jill P., & Tamayo, P. (2015). The Molecular Signatures Database Hallmark Gene Set Collection. *Cell Systems, 1*(6), 417-425. doi:10.1016/j.cels.2015.12.004

Lim, T., Kim, S. J., Kim, K., Lee, J.-I., Lim, D. H., Lee, D. J., . . . Kim, W. S. (2011). Primary CNS lymphoma other than DLBCL: a descriptive analysis of clinical features and treatment outcomes. *Annals of Hematology, 90*(12), 1391-1398. doi:10.1007/s00277-011-1225-0

Lionakis, M. S., Dunleavy, K., Roschewski, M., Widemann, B. C., Butman, J. A., Schmitz, R., . . . Wilson, W. H. (2017). Inhibition of B Cell Receptor Signaling by Ibrutinib in Primary CNS Lymphoma. *Cancer Cell, 31*(6), 833-843.e835. doi:10.1016/j.ccell.2017.04.012

Liu, P., Ge, M., Hu, J., Li, X., Che, L., Sun, K., . . . Chen, X. (2017). A functional mammalian target of rapamycin complex 1 signaling is indispensable for c-Myc-driven hepatocarcinogenesis. *Hepatology, 66*(1), 167-181. doi:10.1002/hep.29183

Loiarro, M., Gallo, G., Fanto, N., De Santis, R., Carminati, P., Ruggiero, V., & Sette, C. (2009). Identification of critical residues of the MyD88 death domain involved in the recruitment of downstream kinases. *J Biol Chem, 284*(41), 28093-28103. doi:10.1074/jbc.M109.004465

Luo, W., Weisel, F., & Shlomchik, M. J. (2018). B Cell Receptor and CD40 Signaling Are Rewired for Synergistic Induction of the c-Myc Transcription Factor in Germinal Center B Cells. *Immunity, 48*(2), 313-326 e315. doi:10.1016/j.immuni.2018.01.008

Maddocks, K. J., Ruppert, A. S., Lozanski, G., Heerema, N. A., Zhao, W., Abruzzo, L., . . . Woyach, J. A. (2015). Etiology of Ibrutinib Therapy Discontinuation and Outcomes in Patients With Chronic Lymphocytic Leukemia. *JAMA Oncology, 1*(1), 80. doi:10.1001/jamaoncol.2014.218

Mamane, Y., Petroulakis, E., LeBacquer, O., & Sonenberg, N. (2006). mTOR, translation initiation and cancer. *Oncogene, 25*(48), 6416-6422. doi:10.1038/sj.onc.1209888

Martin, P., Maddocks, K., Leonard, J. P., Ruan, J., Goy, A., Wagner-Johnston, N., . . . Blum, K. A. (2016). Postibrutinib outcomes in patients with mantle cell lymphoma. *Blood, 127*(12), 1559-1563. doi:10.1182/blood-2015-10-673145

Mato, A. R., Shah, N. N., Jurczak, W., Cheah, C. Y., Pagel, J. M., Woyach, J. A., . . . Wang, M. (2021). Pirtobrutinib in relapsed or refractory B-cell malignancies (BRUIN): a phase 1/2 study. *Lancet, 397*(10277), 892-901. doi:10.1016/S0140-6736(21)00224-5

Mohanty, A., Sandoval, N., Das, M., Pillai, R., Chen, L., Chen, R. W., . . . Ngo, V. N. (2016). CCND1 mutations increase protein stability and promote ibrutinib resistance in mantle cell lymphoma. *Oncotarget, 7*(45), 73558-73572. doi:10.18632/oncotarget.12434

Montesinos-Rongen, M., Purschke, F. G., Brunn, A., May, C., Nordhoff, E., Marcus, K., & Deckert, M. (2015). Primary Central Nervous System (CNS) Lymphoma B Cell Receptors Recognize CNS Proteins. *The Journal of Immunology, 195*(3), 1312-1319. doi:10.4049/jimmunol.1402341

Montesinos-Rongen, M., Van Roost, D., Schaller, C., Wiestler, O. D., & Deckert, M. (2004). Primary diffuse large B-cell lymphomas of the central nervous system are targeted by aberrant somatic hypermutation. *Blood, 103*(5), 1869-1875. doi:10.1182/blood-2003-05-1465

Mootha, V. K., Lindgren, C. M., Eriksson, K. F., Subramanian, A., Sihag, S., Lehar, J., . . . Groop, L. C. (2003). PGC-1alpha-responsive genes involved in oxidative phosphorylation are coordinately downregulated in human diabetes. *Nat Genet, 34*(3), 267-273. doi:10.1038/ng1180

Munshi, M., Liu, X., Chen, J. G., Xu, L., Tsakmaklis, N., Demos, M. G., . . . Yang, G. (2020). SYK is activated by mutated MYD88 and drives pro-survival signaling in MYD88 driven B-cell lymphomas. *Blood Cancer Journal, 10*(1). doi:10.1038/s41408-020-0277-6

Neves, J. F., Doffinger, R., Barcena-Morales, G., Martins, C., Papapietro, O., Plagnol, V., . . . Nejentsev, S. (2018). Novel PLCG2 Mutation in a Patient With APLAID and Cutis Laxa. *Front Immunol, 9*, 2863. doi:10.3389/fimmu.2018.02863

Nitta, N., Nakasu, S., Shima, A., & Nozaki, K. (2016). mTORC1 signaling in primary central nervous system lymphoma. *Surgical Neurology International, 7*(18), 475. doi:10.4103/2152-7806.185781

Notta, F., Mulligan, C. G., Wang, J. C., Poeppl, A., Doulatov, S., Phillips, L. A., . . . Dick, J. E. (2011). Evolution of human BCR-ABL1 lymphoblastic leukaemia-initiating cells. *Nature, 469*(7330), 362-367. doi:10.1038/nature09733

Noy, A., de Vos, S., Thieblemont, C., Martin, P., Flowers, C. R., Morschhauser, F., . . . Chen, R. (2017). Targeting Bruton tyrosine kinase with ibrutinib in relapsed/refractory marginal zone lymphoma. *Blood, 129*(16), 2224-2232. doi:10.1182/blood-2016-10-747345

Nozaki, M., Tada, M., Mizugaki, Y., Takada, K., Nagashima, K., Sawamura, Y., & Abe, H. (1998). Expression of oncogenic molecules in primary central nervous system lymphomas in immunocompetent patients. *Acta Neuropathol, 95*(5), 505-510. doi:10.1007/s004010050831

O'Neill, L. A. J., Golenbock, D., & Bowie, A. G. (2013). The history of Toll-like receptors — redefining innate immunity. *Nature Reviews Immunology, 13*(6), 453-460. doi:10.1038/nri3446

O'Reilly, K. E., Rojo, F., She, Q.-B., Solit, D., Mills, G. B., Smith, D., . . . Rosen, N. (2006). mTOR Inhibition Induces Upstream Receptor Tyrosine Kinase Signaling and Activates Akt. *Cancer Research, 66*(3), 1500-1508. doi:10.1158/0008-5472.can-05-2925

Page, T. H., Urbaniak, A. M., Espirito Santo, A. I., Danks, L., Smallie, T., Williams, L. M., & Horwood, N. J. (2018). Bruton's tyrosine kinase regulates TLR7/8-induced TNF transcription via nuclear factor-kappaB recruitment. *Biochem Biophys Res Commun, 499*(2), 260-266. doi:10.1016/j.bbrc.2018.03.140

Pao, L. I., Famiglietti, S. J., & Cambier, J. C. (1998). Asymmetrical phosphorylation and function of immunoreceptor tyrosine-based activation motif tyrosines in B cell antigen receptor signal transduction. *J Immunol, 160*(7), 3305-3314. Retrieved from https://www.ncbi.nlm.nih.gov/pubmed/9531288

Parray, A., Siddique, H. R., Kuriger, J. K., Mishra, S. K., Rhim, J. S., Nelson, H. H., . . . Saleem, M. (2014). ROBO1, a tumor suppressor and critical molecular barrier for localized tumor cells to acquire invasive phenotype: Study in African-American and Caucasian prostate cancer models. *International Journal of Cancer, 135*(11), 2493-2506. doi:10.1002/ijc.28919

Pasqualucci, L., Neumeister, P., Goossens, T., Nanjangud, G., Chaganti, R. S., Kuppers, R., & Dalla-Favera, R. (2001). Hypermutation of multiple proto-oncogenes in B-cell diffuse large-cell lymphomas. *Nature, 412*(6844), 341-346. doi:10.1038/35085588

Paulus, A., Akhtar, S., Yousaf, H., Manna, A., Paulus, S. M., Bashir, Y., . . . Chanan-Khan, A. (2017). Waldenstrom macroglobulinemia cells devoid of BTKC481S or CXCR4WHIM-like mutations acquire resistance to ibrutinib through upregulation of Bcl-2 and AKT resulting in vulnerability towards venetoclax or MK2206 treatment. *Blood Cancer Journal, 7*(5), e565-e565. doi:10.1038/bcj.2017.40

Phelan, J. D., Young, R. M., Webster, D. E., Roulland, S., Wright, G. W., Kasbekar, M., . . . Staudt, L. M. (2018). A multiprotein supercomplex controlling oncogenic signalling in lymphoma. *Nature, 560*(7718), 387-391. doi:10.1038/s41586-018-0290-0

Pouzoulet, F., Alentorn, A., Royer-Perron, L., Assayag, F., Mokhtari, K., Labiod, D., . . . Soussain, C. (2019). Primary CNS lymphoma patient-derived orthotopic xenograft model capture the biological and molecular characteristics of the disease. *Blood Cells Mol Dis, 75*, 1-10. doi:10.1016/j.bcmd.2018.11.005

Rahal, R., Frick, M., Romero, R., Korn, J. M., Kridel, R., Chun Chan, F., . . . Stegmeier, F. (2013). Pharmacological and genomic profiling identifies NF-κB–targeted treatment strategies for mantle cell lymphoma. *Nature Medicine, 20*(1), 87-92. doi:10.1038/nm.3435

Ravitz, M. J., Chen, L., Lynch, M., & Schmidt, E. V. (2007). c-myc Repression of TSC2 contributes to control of translation initiation and Myc-induced transformation. *Cancer Res, 67*(23), 11209-11217. doi:10.1158/0008-5472.CAN-06-4351

Rendeiro, A. F., Krausgruber, T., Fortelny, N., Zhao, F., Penz, T., Farlik, M., . . . Bock, C. (2020). Chromatin mapping and single-cell immune profiling define the temporal dynamics of ibrutinib response in CLL. *Nature Communications, 11*(1). doi:10.1038/s41467-019-14081-6

Rhee, S. G., & Bae, Y. S. (1997). Regulation of phosphoinositide-specific phospholipase C isozymes. *J Biol Chem, 272*(24), 15045-15048. doi:10.1074/jbc.272.24.15045

Rhyasen, G. W., & Starczynowski, D. T. (2014). IRAK signalling in cancer. *British Journal of Cancer, 112*(2), 232-237. doi:10.1038/bjc.2014.513

Rocha, T. M. B. d. S. d., Fortier, S. C., Pinto, M. S. G., Silva, I. C. d., Paes, R. P., & Chiattone, C. S. (2013). Secondary infiltration of the central nervous system in patients with diffuse large B-cell lymphoma. *Revista Brasileira de Hematologia e Hemoterapia, 35*(4). doi:10.5581/1516-8484.20130094

Rubenstein, J. L., Fridlyand, J., Shen, A., Aldape, K., Ginzinger, D., Batchelor, T., . . . Shuman, M. (2006). Gene expression and angiotropism in primary CNS lymphoma. *Blood, 107*(9), 3716-3723. doi:10.1182/blood-2005-03-0897

Ruland, J., & Hartjes, L. (2018). CARD–BCL-10–MALT1 signalling in protective and pathological immunity. *Nature Reviews Immunology, 19*(2), 118-134. doi:10.1038/s41577-018-0087-2

Saba, N. S., Liu, D., Herman, S. E., Underbayev, C., Tian, X., Behrend, D., . . . Wiestner, A. (2016). Pathogenic role of B-cell receptor signaling and canonical NF-kappaB activation in mantle cell lymphoma. *Blood, 128*(1), 82-92. doi:10.1182/blood-2015-11-681460

Saito, K., Scharenberg, A. M., & Kinet, J. P. (2001). Interaction between the Btk PH domain and phosphatidylinositol-3,4,5-trisphosphate directly regulates Btk. *J Biol Chem, 276*(19), 16201-16206. doi:10.1074/jbc.M100873200

Sarbassov, D. D., Guertin, D. A., Ali, S. M., & Sabatini, D. M. (2005). Phosphorylation and regulation of Akt/PKB by the rictor-mTOR complex. *Science, 307*(5712), 1098-1101. doi:10.1126/science.1106148

Schaff, L. R., Ambady, P., Doolittle, N. D., & Grommes, C. (2021). Primary central nervous system lymphoma: a narrative review of ongoing clinical

trials and goals for future studies. *Annals of Lymphoma, 5*, 8-8. doi:10.21037/aol-20-47

Schafflick, D., Wolbert, J., Heming, M., Thomas, C., Hartlehnert, M., Borsch, A. L., . . . Meyer Zu Horste, G. (2021). Single-cell profiling of CNS border compartment leukocytes reveals that B cells and their progenitors reside in non-diseased meninges. *Nat Neurosci*. doi:10.1038/s41593-021-00880-y

Schauer, S. L., Wang, Z., Sonenshein, G. E., & Rothstein, T. L. (1996). Maintenance of nuclear factor-kappa B/Rel and c-myc expression during CD40 ligand rescue of WEHI 231 early B cells from receptor-mediated apoptosis through modulation of I kappa B proteins. *J Immunol, 157*(1), 81-86. Retrieved from https://www.ncbi.nlm.nih.gov/pubmed/8683159

Schmidt, E. V. (2004). The role of c-myc in regulation of translation initiation. *Oncogene, 23*(18), 3217-3221. doi:10.1038/sj.onc.1207548

Schmitz, R., Wright, G. W., Huang, D. W., Johnson, C. A., Phelan, J. D., Wang, J. Q., . . . Staudt, L. M. (2018). Genetics and Pathogenesis of Diffuse Large B-Cell Lymphoma. *New England Journal of Medicine, 378*(15), 1396-1407. doi:10.1056/NEJMoa1801445

Schneider, C., Pasqualucci, L., & Dalla-Favera, R. (2011). Molecular pathogenesis of diffuse large B-cell lymphoma. *Semin Diagn Pathol, 28*(2), 167-177. doi:10.1053/j.semdp.2011.04.001

Sharma, S., Galanina, N., Guo, A., Lee, J., Kadri, S., Van Slambrouck, C., . . . Wang, Y. L. (2016). Identification of a structurally novel BTK mutation that drives ibrutinib resistance in CLL. *Oncotarget, 7*(42), 68833-68841. doi:10.18632/oncotarget.11932

Son, S.-M., Ha, S.-Y., Yoo, H.-Y., Oh, D., Kim, S.-J., Kim, W.-S., & Ko, Y.-H. (2016). Prognostic impact of MYC protein expression in central nervous system diffuse large B-cell lymphoma: comparison with MYC rearrangement and MYC mRNA expression. *Modern Pathology, 30*(1), 4-14. doi:10.1038/modpathol.2016.56

Song, Y., Zhou, K., Zou, D., Zhou, J., Hu, J., Yang, H., . . . Zhu, J. (2020). Treatment of Patients with Relapsed or Refractory Mantle–Cell Lymphoma with Zanubrutinib, a Selective Inhibitor of Bruton's Tyrosine Kinase. *Clinical Cancer Research, 26*(16), 4216-4224. doi:10.1158/1078-0432.ccr-19-3703

Srinivasan, L., Sasaki, Y., Calado, D. P., Zhang, B., Paik, J. H., DePinho, R. A., . . . Rajewsky, K. (2009). PI3 kinase signals BCR-dependent mature B cell survival. *Cell, 139*(3), 573-586. doi:10.1016/j.cell.2009.08.041

Subramanian, A., Tamayo, P., Mootha, V. K., Mukherjee, S., Ebert, B. L., Gillette, M. A., . . . Mesirov, J. P. (2005). Gene set enrichment analysis: A knowledge-based approach for interpreting genome-wide expression profiles. *Proceedings of the National Academy of Sciences, 102*(43), 15545-15550. doi:10.1073/pnas.0506580102

Tateishi, K., Miyake, Y., Kawazu, M., Sasaki, N., Nakamura, T., Sasame, J., . . . Yamamoto, T. (2020). A Hyperactive RelA/p65-Hexokinase 2 Signaling

Axis Drives Primary Central Nervous System Lymphoma. *Cancer Research, 80*(23), 5330-5343. doi:10.1158/0008-5472.can-20-2425

Treon, S. P., Tripsas, C. K., Meid, K., Warren, D., Varma, G., Green, R., . . . Advani, R. H. (2015). Ibrutinib in Previously Treated Waldenström's Macroglobulinemia. *New England Journal of Medicine, 372*(15), 1430-1440. doi:10.1056/NEJMoa1501548

Uccelli, A., Aloisi, F., & Pistoia, V. (2005). Unveiling the enigma of the CNS as a B-cell fostering environment. *Trends in Immunology, 26*(5), 254-259. doi:10.1016/j.it.2005.02.009

Wall, M., Poortinga, G., Hannan, K. M., Pearson, R. B., Hannan, R. D., & McArthur, G. A. (2008). Translational control of c-MYC by rapamycin promotes terminal myeloid differentiation. *Blood, 112*(6), 2305-2317. doi:10.1182/blood-2007-09-111856

Wang, L., Harris, T. E., Roth, R. A., & Lawrence, J. C. (2007). PRAS40 Regulates mTORC1 Kinase Activity by Functioning as a Direct Inhibitor of Substrate Binding. *Journal of Biological Chemistry, 282*(27), 20036-20044. doi:10.1074/jbc.M702376200

Wang, M., Rule, S., Zinzani, P. L., Goy, A., Casasnovas, O., Smith, S. D., . . . Jurczak, W. (2018). Acalabrutinib in relapsed or refractory mantle cell lymphoma (ACE-LY-004): a single-arm, multicentre, phase 2 trial. *The Lancet, 391*(10121), 659-667. doi:10.1016/s0140-6736(17)33108-2

Wang, M. L., Rule, S., Martin, P., Goy, A., Auer, R., Kahl, B. S., . . . Blum, K. A. (2013). Targeting BTK with Ibrutinib in Relapsed or Refractory Mantle-Cell Lymphoma. *New England Journal of Medicine, 369*(6), 507-516. doi:10.1056/NEJMoa1306220

Wang, Z., Hutcherson, S. M., Yang, C., Jattani, R. P., Tritapoe, J. M., Yang, Y. K., & Pomerantz, J. L. (2019). Coordinated regulation of scaffold opening and enzymatic activity during CARD11 signaling. *J Biol Chem, 294*(40), 14648-14660. doi:10.1074/jbc.RA119.009551

Watt, S. A., Purdie, K. J., den Breems, N. Y., Dimon, M., Arron, S. T., McHugh, A. T., . . . South, A. P. (2015). Novel CARD11 Mutations in Human Cutaneous Squamous Cell Carcinoma Lead to Aberrant NF-κB Regulation. *The American Journal of Pathology, 185*(9), 2354-2363. doi:10.1016/j.ajpath.2015.05.018

Wilson, W. H., Young, R. M., Schmitz, R., Yang, Y., Pittaluga, S., Wright, G., . . . Staudt, L. M. (2015). Targeting B cell receptor signaling with ibrutinib in diffuse large B cell lymphoma. *Nature Medicine, 21*(8), 922-926. doi:10.1038/nm.3884

Woyach, J. A., Furman, R. R., Liu, T. M., Ozer, H. G., Zapatka, M., Ruppert, A. S., . . . Byrd, J. C. (2014). Resistance mechanisms for the Bruton's tyrosine kinase inhibitor ibrutinib. *N Engl J Med, 370*(24), 2286-2294. doi:10.1056/NEJMoa1400029

Woyach, J. A., Ruppert, A. S., Guinn, D., Lehman, A., Blachly, J. S., Lozanski, A., . . . Byrd, J. C. (2017). BTK(C481S)-Mediated Resistance to Ibrutinib in Chronic Lymphocytic Leukemia. *J Clin Oncol, 35*(13), 1437-1443. doi:10.1200/JCO.2016.70.2282

Wright, G. W., Huang, D. W., Phelan, J. D., Coulibaly, Z. A., Roulland, S., Young, R. M., . . . Staudt, L. M. (2020). A Probabilistic Classification Tool for Genetic Subtypes of Diffuse Large B Cell Lymphoma with Therapeutic Implications. *Cancer Cell, 37*(4), 551-568.e514. doi:10.1016/j.ccell.2020.03.015

Wu, C., de Miranda, N. F., Chen, L., Wasik, A. M., Mansouri, L., Jurczak, W., . . . Pan-Hammarstrom, Q. (2016). Genetic heterogeneity in primary and relapsed mantle cell lymphomas: Impact of recurrent CARD11 mutations. *Oncotarget, 7*(25), 38180-38190. doi:10.18632/oncotarget.9500

Xu, L., Tsakmaklis, N., Yang, G., Chen, J. G., Liu, X., Demos, M., . . . Treon, S. P. (2017). Acquired mutations associated with ibrutinib resistance in Waldenstrom macroglobulinemia. *Blood, 129*(18), 2519-2525. doi:10.1182/blood-2017-01-761726

Xu, Y., Harder, K. W., Huntington, N. D., Hibbs, M. L., & Tarlinton, D. M. (2005). Lyn Tyrosine Kinase. *Immunity, 22*(1), 9-18. doi:10.1016/j.immuni.2004.12.004

Yang, G., Zhou, Y., Liu, X., Xu, L., Cao, Y., Manning, R. J., . . . Treon, S. P. (2013). A mutation in MYD88 (L265P) supports the survival of lymphoplasmacytic cells by activation of Bruton tyrosine kinase in Waldenstrom macroglobulinemia. *Blood, 122*(7), 1222-1232. doi:10.1182/blood-2012-12-475111

Yang, Y.-K., Yang, C., Chan, W., Wang, Z., Deibel, K. E., & Pomerantz, J. L. (2016). Molecular Determinants of Scaffold-induced Linear Ubiquitinylation of B Cell Lymphoma/Leukemia 10 (Bcl10) during T Cell Receptor and Oncogenic Caspase Recruitment Domain-containing Protein 11 (CARD11) Signaling. *Journal of Biological Chemistry, 291*(50), 25921-25936. doi:10.1074/jbc.M116.754028

Yin, W., Xia, X., Wu, M., Yang, H., Zhu, X., Sun, W., & Ge, M. (2019). The impact of BCL-2/MYC protein expression and gene abnormality on primary central nervous system diffuse large B-cell lymphoma. *Int J Clin Exp Pathol, 12*(6), 2215-2223. Retrieved from https://www.ncbi.nlm.nih.gov/pubmed/31934044

Zhang, L., Yao, Y., Zhang, S., Liu, Y., Guo, H., Ahmed, M., . . . Wang, M. (2019). Metabolic reprogramming toward oxidative phosphorylation identifies a therapeutic target for mantle cell lymphoma. *Sci Transl Med, 11*(491). doi:10.1126/scitranslmed.aau1167

Zhang, Q., Lenardo, M. J., & Baltimore, D. (2017). 30 Years of NF-κB: A Blossoming of Relevance to Human Pathobiology. *Cell, 168*(1-2), 37-57. doi:10.1016/j.cell.2016.12.012

Zhao, X., Lwin, T., Silva, A., Shah, B., Tao, J., Fang, B., . . . Tao, J. (2017). Unification of de novo and acquired ibrutinib resistance in mantle cell lymphoma. *Nature Communications, 8*(1). doi:10.1038/ncomms14920